



Orthogonal spline expansions for uncertainty quantification in linear dynamical systems[☆]

Sharif Rahman^{*,1}, Ramin Jahanbin

College of Engineering, The University of Iowa, Iowa City, IA 52242, USA

ARTICLE INFO

Keywords:

B-splines
Frequency response function
Polynomial chaos expansion
Random eigenvalue problem
Spline chaos expansion
Spline dimensional decomposition

ABSTRACT

This paper leverages recent progress on orthonormal splines for solving uncertainty quantification (UQ) problems from linear structural dynamics. The resulting methods, premised on spline chaos expansion (SCE) and spline dimensional decomposition (SDD), both construe Fourier-like expansion of a dynamic system response of interest with respect to measure-consistent orthonormalized basis splines in input random variables and standard least-squares regression for estimating the expansion coefficients. The SCE and SDD methods are capable of capturing high nonlinearity and non-smoothness, if they exist, in a stochastic dynamic response markedly better than the polynomial chaos expansion (PCE) method. However, due to the tensor-product structure, SCE, like PCE, also suffers from the curse of dimensionality. In contrast, SDD, equipped with a desirable dimensional hierarchy of input variables, deflates the curse of dimensionality to a great extent. Numerical results from frequency response analysis of a two-degree-of-freedom dynamic system indicate that a low-order SCE with fewer basis functions removes or markedly reduces the spurious oscillations generated by high-order PCE in estimating the response statistics. Finally, a high-dimensional modal analysis of a fighter jet comprising 110 random variables was conducted, demonstrating the ability of SDD in solving large-scale UQ problems.

1. Introduction

Computational modeling and simulation of complex dynamical systems in engineering and applied sciences often mandate uncertainty quantification (UQ) due to the natural variability of system properties, external excitations, and initial/boundary conditions [1,2]. The propagation of uncertainties from the input to the output of a dynamic system is commonly associated with the sampling-based methods, for instance, Monte Carlo simulation (MCS), which are robust but not suitable when only a small number of full-scale dynamic simulations are manageable. As a result, UQ is now witnessing a massive surge in the development of surrogate or approximate computational methods with the goal of achieving risk mitigation through scientific prediction. Indeed, there exists a myriad of UQ methods, namely, polynomial chaos expansion (PCE) [3,4], polynomial dimensional decomposition (PDD) [5,6], the stochastic collocation methods [7,8], and sparse-grid quadrature [9,10], which are often viewed as surrogates for expensive-to-run MCS and its variants [11,12]. These methods and a few others not explicitly stated here for brevity, while successful in conducting UQ analysis of quasi-static problems, are known to face severe technical hurdles when dealing with time-dependent or stochastic-dynamics problems [13–15]. In addition, most existing methods begin to break down for truly high-dimensional problems,

[☆] Grant sponsor: U.S. National Science Foundation; Grant Nos. CMMI-1607398, CMMI-1933114.

* Corresponding author.

E-mail addresses: sharif-rahman@uiowa.edu (S. Rahman), ramin-jahanbin@uiowa.edu (R. Jahanbin).

¹ Professor.

List of abbreviations

CDF	Cumulative distribution function
COV	Coefficient of variation
FEA	Finite-element analysis
FRF	Frequency response function
MCS	Monte Carlo simulation
PCE	Polynomial chaos expansion
PDD	Polynomial dimensional decomposition
PDF	Probability density function
SCE	Spline chaos expansion
SDD	Spline dimensional decomposition
SLS	Standard least-squares
UQ	Uncertainty quantification

where hundreds of input random variables are necessary to characterize dynamic system states and forecast their evolution in time. Therefore, development of new surrogate methods capable of effectively handling high-dimensional stochastic-dynamics problems is desirable.

For linear systems subject to harmonic excitations, determining frequency response functions (FRFs) is a fundamental task in structural dynamics. They provide valuable dynamic response characteristics over a frequency range with a clear physical interpretation. However, due to possible uncertainty in mass, damping, and stiffness properties, FRFs are actually random functions, requiring evaluation of their probabilistic attributes. Relevant works entail mode-based meta models for probabilistic analysis of FRFs [16], modal approaches for stochastic dynamic analysis in the frequency domain [17], and polynomial expansion leading to bounds of statistical properties of FRFs [18], to name a few. Later on, Kundu and Adhikari [19] obtained FRFs of a stochastic system by projecting the response on a reduced subspace of eigenvectors. A few additional studies employing PCE as the surrogate method of UQ analysis have also been reported. For instance, Jacquelin et al. [20] exploited PCE in calculating the second-moment statistics of FRFs for a two-degree-of-freedom system. They reported spurious oscillations generated by standard PCE around resonant frequencies. The problem becomes further compounded when the uncertainty in the system properties causes the randomness of natural frequencies. Through numerical experiments, they showed that the PCE approximations converge very slowly, requiring impractically large expansion orders to produce satisfactory estimates of the second-moment properties of FRF. Their subsequent work involved convergence acceleration of PCE using Aitken's transformation [21]. A more recent work on PCE consists of a transformation of FRF, where the expansion is applied on a scaled frequency axis [22]. While these latter works helped in resolving some of the PCE-related issues, UQ methods exploiting basis functions more powerful than polynomials have yet to materialize.

Another prominent topic in UQ for dynamic systems is solving random eigenvalue problems. The fundamental objective of random eigenvalue analysis is to characterize quantitatively the uncertainty of the natural frequencies and mode shapes from the known probability distribution of mass, damping, and stiffness properties. Classical methods for solving random eigenvalue problems are dominated by the perturbation method [23], a long-standing staple, but no longer contemporary, as it is restricted to problems with small uncertainties or small nonlinearities. Other methods include the iteration method [23], the Ritz method [24], the crossing theory [25], PCE [26], and PDD [27,28], to mention just five. Moreover, the foregoing stochastic collocation and sparse-grid quadrature can be applied to solve random eigenvalue problems. All of these methods are known to offer significant computational advantages over MCS. However, for truly high-dimensional problems, the PCE or collocation methods require astronomically large numbers of basis functions, succumbing to the curse of dimensionality [29]. Although basis splines (B-splines) have been employed to construct the sparse-grid quadrature, they are neither orthogonal nor measure-consistent, meaning that the underlying basis functions are not adapted to the probability measure of input random variables. While PDD is known to reduce PCE's computational cost to a significant margin [30], both expansions, founded on globally supported polynomial basis, are largely predicated on the smoothness assumption of the output function. For oscillatory, non-smooth, or discontinuous responses, PDD also requires overly large expansion orders, causing unreliable predictions of stochastic performance. This is chiefly because polynomials, being too smooth, are susceptible to unstable swings when the expansion order exceeds four or five [31]. The authors contend that alternative expansions, such as those rooted in low-order splines, should be exploited to generate an accurate but practical way of solving random eigenvalue problems. The rationale for selecting locally supported splines over globally supported polynomials stems from the argument that a highly nonlinear or non-smooth stochastic response, be it an eigenvalue or an eigenfunction, is better suited to be picked up accurately by the former, which comprises smoothly connected locally polynomial functions.

The principal objective of this study is to introduce two novel expansions, referred to as spline chaos expansion (SCE) and spline dimensional decomposition (SDD), for solving UQ problems in structural dynamics involving frequency response analysis and modal analysis. While this paper focuses on the computational and practical aspects of the expansions, readers interested in rigorous mathematical analyses of SCE and SDD, including theoretical results and their formal proofs, should consult the respective prequels [32,33]. The paper is organized as follows. Section 2 begins with mathematical preliminaries and requisite assumptions. Section 3 presents a problem description for each class of UQ analysis addressed in this work, leading to a consolidated

general problem statement. Section 4 describes the construction of measure-consistent, univariate orthonormalized B-splines in each coordinate direction. Section 5 introduces SCE and SDD for a square-integrable output random variable of interest, including the approximations or methods emanating from their truncations. In the same section, analytical formulae for the mean and variance of a truncated SCE/SDD are derived. The calculation of the SCE/SDD coefficients is discussed in Section 6. Two numerical examples, one focusing on the FRFs of two-degree-of-freedom dynamic systems and the other entailing the natural frequencies and mode shapes of a 110-dimensional, industrial-scale engineering problem, are provided in Section 7. Finally, conclusions are drawn in Section 8.

2. Input random variables and dynamic system matrices

Let $\mathbb{N} := \{1, 2, \dots\}$, $\mathbb{N}_0 := \mathbb{N} \cup \{0\}$, $\mathbb{R} := (-\infty, +\infty)$, $\mathbb{R}_0^+ := [0, +\infty)$, $\mathbb{R}^+ := (0, +\infty)$, and \mathbb{C} be the sets of positive integers (natural), non-negative integers, all real numbers, non-negative real numbers, positive real numbers, and complex numbers, respectively. Denote by $[a_k, b_k]$ a finite closed interval, where $a_k, b_k \in \mathbb{R}$ and $b_k > a_k$. Then, given $N \in \mathbb{N}$, $\mathbb{A}^N = \times_{k=1}^N [a_k, b_k]$ represents a closed bounded domain of \mathbb{R}^N .

Let $(\Omega, \mathcal{F}, \mathbb{P})$ be a probability space, where Ω is a sample space representing an abstract set of elementary events, \mathcal{F} is a σ -algebra on Ω , and $\mathbb{P} : \mathcal{F} \rightarrow [0, 1]$ is a probability measure. Defined on this probability space, consider an N -dimensional input random vector $\mathbf{X} := (X_1, \dots, X_N)^T$, describing the statistical uncertainties in the mass, damping, and stiffness properties of a linear dynamic system. Denote by $F_{\mathbf{X}}(\mathbf{x}) := \mathbb{P}(\cap_{i=1}^N \{X_i \leq x_i\})$ the joint cumulative distribution function (CDF) of \mathbf{X} . The k th component of \mathbf{X} is a random variable X_k , which has the marginal CDF $F_{X_k}(x_k) := \mathbb{P}(X_k \leq x_k)$. The positive integer N , which represents the total number of input random variables, is often referred to as the dimension of the stochastic or UQ problem.

For $M \in \mathbb{N}$, consider a linear, M -degree-of-freedom, dynamic system with random mass matrix $\mathbf{M}(\mathbf{X}) \in \mathbb{R}^{M \times M}$, random damping matrix $\mathbf{C}(\mathbf{X}) \in \mathbb{R}^{M \times M}$, and random stiffness matrix $\mathbf{K}(\mathbf{X}) \in \mathbb{R}^{M \times M}$. The probabilistic characteristics of these system matrices are derived from the probability law of \mathbf{X} . As an example, consider a mass–spring–damper model of a single-degree-of-freedom dynamic system with mass M , damping coefficient C , and spring constant K . If all of these input parameters are modeled as random variables, then $\mathbf{X} := (M, C, K)^T$ with stochastic dimension $N = 3$.

The requisite assumptions on input random variables and dynamic system matrices are as follows.

Assumption 1. The input random vector $\mathbf{X} := (X_1, \dots, X_N)^T$ satisfies all of the following conditions:

- (1) All component random variables X_k , $k = 1, \dots, N$, are statistically independent, but not necessarily identically distributed.
- (2) Each input random variable X_k is defined on a bounded interval $[a_k, b_k] \subset \mathbb{R}$. Therefore, all moments of X_k exist, that is, for all $l \in \mathbb{N}$,

$$\mathbb{E} [X_k^l] := \int_{\Omega} X_k^l(\omega) d\mathbb{P}(\omega) < \infty, \tag{1}$$

where \mathbb{E} is the expectation operator with respect to the probability measure \mathbb{P} .

- (3) Each input random variable X_k has absolutely continuous marginal CDF $F_{X_k}(x_k)$ and continuous marginal probability density function (PDF) $f_{X_k}(x_k) := \partial F_{X_k}(x_k) / \partial x_k$ with a bounded support $[a_k, b_k] \subset \mathbb{R}$. Consequently, with Items (1) and (2) in mind, the joint CDF $F_{\mathbf{X}}(\mathbf{x})$ and joint PDF $f_{\mathbf{X}}(\mathbf{x}) := \partial^N F_{\mathbf{X}}(\mathbf{x}) / \partial x_1 \dots \partial x_N$ of \mathbf{X} are obtained from

$$F_{\mathbf{X}}(\mathbf{x}) = \prod_{k=1}^N F_{X_k}(x_k) \text{ and } f_{\mathbf{X}}(\mathbf{x}) = \prod_{k=1}^N f_{X_k}(x_k), \tag{2}$$

respectively, with a bounded support $\mathbb{A}^N \subset \mathbb{R}^N$ of the density function.

Assumption 2. The dynamic system matrices fulfill all of the following conditions:

- (1) The mass matrix $\mathbf{M}(\mathbf{X})$ is real, symmetric, and positive-definite, whereas the stiffness matrix $\mathbf{K}(\mathbf{X})$ and damping matrix $\mathbf{C}(\mathbf{X})$ are real, symmetric, and positive semi-definite.
- (2) The damping matrix $\mathbf{C}(\mathbf{X})$ can be proportional or non-proportional. If proportional, the damping matrix is a linear combination of the mass and stiffness matrices.

Assumption 1 ensures the existence of a relevant sequence of orthogonal polynomials or splines consistent with the input probability measure. **Assumption 2** guarantees real-valued eigensolutions for undamped or proportionally damped systems. For non-proportionally damped systems, the eigensolutions can be real-valued or complex-valued, depending on the damping matrix.

3. UQ problems in structural dynamics

Consider a linear, M -degree-of-freedom, dynamic system with random mass matrix $\mathbf{M}(\mathbf{X}) \in \mathbb{R}^{M \times M}$, random damping matrix $\mathbf{C}(\mathbf{X}) \in \mathbb{R}^{M \times M}$, and random stiffness matrix $\mathbf{K}(\mathbf{X}) \in \mathbb{R}^{M \times M}$, satisfying **Assumption 2**. Under external excitation with an M -dimensional deterministic force vector $\mathbf{f}(t)$, the governing equation of motion in the time domain is

$$\mathbf{M}(\mathbf{X})\ddot{\mathbf{z}}(t; \mathbf{X}) + \mathbf{C}(\mathbf{X})\dot{\mathbf{z}}(t; \mathbf{X}) + \mathbf{K}(\mathbf{X})\mathbf{z}(t; \mathbf{X}) = \mathbf{f}(t), \tag{3}$$

where $t \in [0, T] \subseteq \mathbb{R}_0^+$, $T \in \mathbb{R}^+$, is time, $\mathbf{z}(t; \mathbf{X})$ is the M -dimensional displacement vector, $\dot{\mathbf{z}}(t; \mathbf{X})$ is the M -dimensional velocity vector, and $\ddot{\mathbf{z}}(t; \mathbf{X})$ is the M -dimensional acceleration vector. The second arguments of the displacement, velocity, and acceleration responses indicate that they also depend on the input random vector \mathbf{X} . Two prominent UQ problems from structural dynamics in conjunction with frequency response analysis and modal analysis are described as follows.

3.1. Frequency response analysis

Consider a deterministic harmonic excitation with the complex-valued force vector

$$\mathbf{f}(t) = \mathbf{F}(\omega) \exp(i\omega t), \quad (4)$$

where $i = \sqrt{-1}$, $\omega \in [\omega_l, \omega_r] \subseteq \mathbb{R}^+$, $0 \leq \omega_l < \omega_r < \infty$, is the excitation (angular) frequency, and $\mathbf{F}(\omega) \in \mathbb{R}^M$ is the real-valued force amplitude vector. For a linear system, the steady-state displacement response is

$$\mathbf{z}(t; \mathbf{X}) = \mathbf{Z}(\omega; \mathbf{X}) \exp(i\omega t), \quad (5)$$

where $\mathbf{Z}(\omega; \mathbf{X}) \in \mathbb{C}^M$ is the complex-valued displacement amplitude vector that also depends on \mathbf{X} . It is elementary to show that $\mathbf{Z}(\omega; \mathbf{X})$ satisfies

$$[-\omega^2 \mathbf{M}(\mathbf{X}) + i\omega \mathbf{C}(\mathbf{X}) + \mathbf{K}(\mathbf{X})] \mathbf{Z}(\omega; \mathbf{X}) = \mathbf{F}(\omega), \quad (6)$$

the governing equation of motion in frequency domain. Inverting Eq. (6), the displacement amplitude

$$\mathbf{Z}(\omega; \mathbf{X}) = [-\omega^2 \mathbf{M}(\mathbf{X}) + i\omega \mathbf{C}(\mathbf{X}) + \mathbf{K}(\mathbf{X})]^{-1} \mathbf{F}(\omega) = \mathbf{H}(\omega; \mathbf{X}) \mathbf{F}(\omega), \quad (7)$$

where, in the second equality,

$$\mathbf{H}(\omega; \mathbf{X}) := [-\omega^2 \mathbf{M}(\mathbf{X}) + i\omega \mathbf{C}(\mathbf{X}) + \mathbf{K}(\mathbf{X})]^{-1} \in \mathbb{C}^{M \times M} \quad (8)$$

defines a matrix of complex-valued FRFs for the dynamic system. In UQ analysis, one is interested in propagating the uncertainty of input \mathbf{X} to FRFs, leading to the probabilistic characterization of $\mathbf{Z}(\omega; \mathbf{X})$.

Consider a special case where the i th component of $\mathbf{F}(\omega)$ is *one* and other components are *zero*. Then, from Eq. (7), the i th component of $\mathbf{Z}(\omega; \mathbf{X})$, denoted by $Z_i(\omega; \mathbf{X}) \in \mathbb{C}$, is

$$Z_i(\omega; \mathbf{X}) = H_{ii}(\omega; \mathbf{X}), \quad i = 1, \dots, M, \quad (9)$$

where $H_{ii}(\omega; \mathbf{X}) \in \mathbb{C}$ is the i th diagonal element of $\mathbf{H}(\omega; \mathbf{X})$. Define by

$$|Z_i(\omega; \mathbf{X})| := |H_{ii}(\omega; \mathbf{X})| := \sqrt{[\operatorname{Re}(H_{ii}(\omega; \mathbf{X}))]^2 + [\operatorname{Im}(H_{ii}(\omega; \mathbf{X}))]^2}, \quad i = 1, \dots, M, \quad (10)$$

the modulus or magnitude of $Z_i(\omega; \mathbf{X})$ or $H_{ii}(\omega; \mathbf{X})$ with $\operatorname{Re}(\cdot)$ and $\operatorname{Im}(\cdot)$ representing, respectively, the real and imaginary parts. Here, UQ for frequency response analysis is aimed at calculating the probabilistic characteristics of $|H_{ii}(\omega; \mathbf{X})|$ when the input uncertainty is arbitrarily prescribed, provided that Assumptions 1 and 2 are fulfilled.

According to Eq. (10), only the point FRFs have been considered. The extension to the analysis of cross FRFs is trivial.

3.2. Modal analysis

Consider, again, an M -degree-of-freedom, dynamic system with the system matrices $\mathbf{M}(\mathbf{X})$, $\mathbf{C}(\mathbf{X})$, and $\mathbf{K}(\mathbf{X})$ defined earlier and a general nonlinear function f . The probabilistic characteristics of the system matrices can be derived from the known probability law of \mathbf{X} . A non-trivial solution of

$$f(\lambda(\mathbf{X}); \mathbf{M}(\mathbf{X}), \mathbf{C}(\mathbf{X}), \mathbf{K}(\mathbf{X})) \boldsymbol{\phi}(\mathbf{X}) = \mathbf{0}, \quad (11)$$

if it exists, defines the random eigenvalue $\lambda(\mathbf{X}) \in \mathbb{R}$ or \mathbb{C} and the random eigenvector $\boldsymbol{\phi}(\mathbf{X}) \in \mathbb{R}^M$ or \mathbb{C}^M of a general nonlinear eigenvalue problem. Depending on the applications, a wide variety of functions f and, hence, eigenvalue problems exists. Table 1, reported by Rahman and Yadav [30], lists a few examples of random eigenvalue problems frequently encountered in dynamic systems. Two prominent examples are a linear eigenvalue problem associated with an undamped or proportionally damped system and a quadratic eigenvalue problem affiliated with a non-proportionally damped system. Other types of nonlinear eigenvalue problems, such as palindromic, polynomial, and rational eigenvalue problems, may appear in various applications, where additional system matrices are involved. In the latter cases, dedicated eigenvalue solvers must be used to find a solution, as discussed in modal analysis of viscoelastic sandwich plates [34]. In this work, only linear or quadratic eigenvalue problems are considered.

In general, the eigensolutions depend on the random input \mathbf{X} via solution of the matrix characteristic equation

$$\det [f(\lambda(\mathbf{X}); \mathbf{M}(\mathbf{X}), \mathbf{C}(\mathbf{X}), \mathbf{K}(\mathbf{X}))] = 0 \quad (12)$$

and subsequent solution of Eq. (11). A principal objective in solving a random eigenvalue problem is to determine the probabilistic characteristics of eigenpairs

$$\{\lambda^{(i)}(\mathbf{X}), \boldsymbol{\phi}^{(i)}(\mathbf{X})\}, \quad i = 1, \dots, M,$$

from the known probability distribution of the input random vector \mathbf{X} . For an undamped linear dynamic system, the natural frequencies are the square-root of eigenvalues, whereas the mode shapes are the same as the eigenvectors.

Once the random eigenvalues $\lambda^{(i)}(\mathbf{X})$ and random eigenvectors $\boldsymbol{\phi}^{(i)}(\mathbf{X})$ are determined, say, for a proportionally damped system, they can be used for either time domain or frequency domain analysis. For time domain analysis, the displacement vector $\mathbf{z}(t; \mathbf{X})$

Table 1
Random eigenvalue problems in dynamical systems [30].

Eigenvalue problem ^a	Problem type and application(s)
$[-\lambda(\mathbf{X})\mathbf{M}(\mathbf{X}) + \mathbf{K}(\mathbf{X})] \boldsymbol{\phi}(\mathbf{X}) = \mathbf{0}$	<i>Linear</i> ; undamped or proportionally damped systems
$[\lambda^2(\mathbf{X})\mathbf{M}(\mathbf{X}) + \lambda(\mathbf{X})\mathbf{C}(\mathbf{X}) + \mathbf{K}(\mathbf{X})] \boldsymbol{\phi}(\mathbf{X}) = \mathbf{0}$	<i>Quadratic</i> ; non-proportionally damped systems, singularity problems
$[\lambda(\mathbf{X})\mathbf{M}_1(\mathbf{X}) + \mathbf{M}_0(\mathbf{X}) + \mathbf{M}_1^t(\mathbf{X})/\lambda(\mathbf{X})] \boldsymbol{\phi}(\mathbf{X}) = \mathbf{0}$	<i>Palindromic</i> ; acoustic emissions in high-speed trains
$\left[\sum_k \lambda^k(\mathbf{X})\mathbf{A}_k(\mathbf{X}) \right] \boldsymbol{\phi}(\mathbf{X}) = \mathbf{0}$	<i>Polynomial</i> ; control and dynamics problems
$\left[\lambda(\mathbf{X})\mathbf{M}(\mathbf{X}) - \mathbf{K}(\mathbf{X}) + \sum_k \frac{\lambda^q(\mathbf{X})\mathbf{C}_k(\mathbf{X})}{a_k - \lambda(\mathbf{X})} \right] \boldsymbol{\phi}(\mathbf{X}) = \mathbf{0}$	<i>Rational</i> ; plate vibration ($q = 1$), fluid-structure vibration ($q = 2$), vibration of viscoelastic materials

^a $\mathbf{M}(\mathbf{X})$, $\mathbf{C}(\mathbf{X})$, and $\mathbf{K}(\mathbf{X})$ are mass, damping, stiffness matrices, respectively; $\mathbf{M}_0(\mathbf{X})$, $\mathbf{M}_1(\mathbf{X})$, $\mathbf{A}_k(\mathbf{X})$, and $\mathbf{C}_k(\mathbf{X})$ are various coefficient matrices.

is obtained from the linear transformation $\mathbf{z}(t; \mathbf{X}) = \boldsymbol{\Phi}(\mathbf{X})\mathbf{q}(t; \mathbf{X})$, where $\mathbf{q}(t; \mathbf{X}) \in \mathbb{R}^M$ is the vector of normal coordinates and $\boldsymbol{\Phi}(\mathbf{X}) \in \mathbb{R}^{M \times M}$ is the matrix of M random eigenvectors as its columns. Due to proportional damping, the governing equations for a multi-degree-of-freedom system are uncoupled in normal coordinates, thus obtaining $\mathbf{q}(t; \mathbf{X})$ by solving a series of governing ordinary differential equations for single-degree-of-freedom systems. For frequency domain analysis, under the assumption of viscous damping and mass-normalized eigenvectors, an FRF can also be expressed as a nonlinear function of natural frequencies, mode shapes, and modal damping. Therefore, the solution of random eigenvalue problems has several applications in stochastic dynamic analysis.

3.3. A general problem statement

Given an input random vector $\mathbf{X} := (X_1, \dots, X_N)^T : (\Omega, \mathcal{F}) \rightarrow (\mathbb{A}^N, \mathcal{B}^N)$ with known PDF $f_{\mathbf{X}}(\mathbf{x})$ on $\mathbb{A}^N \subset \mathbb{R}^N$, denote by $y(\mathbf{X}) := y(X_1, \dots, X_N)$ a real-valued, measurable transformation on (Ω, \mathcal{F}) , describing a general output response of a stochastic dynamic system. For instance, $y(\mathbf{X}) = |H_{ii}(\omega; \mathbf{X})|$ from frequency response analysis in Eq. (10); or $y(\mathbf{X}) = \lambda(\mathbf{X})$ from eigenvalue analysis in Eq. (12). For eigenvalue analysis, $y(\mathbf{X})$ may also represent any component of the eigenvector $\boldsymbol{\phi}(\mathbf{X})$ in Eq. (11), provided that a consistent normalization of the mode shape is employed. If the eigensolutions are complex-valued, then $y(\mathbf{X})$ represents either the real or imaginary parts of eigenvalues and eigenvectors. Regardless of which stochastic-dynamics problem is being solved, the output function y is implicit, is not analytically available, and can only be viewed as a high-dimensional input–output mapping, where the evaluation of the output function y for a given sample input \mathbf{x} requires expensive finite-element analysis (FEA). A major objective of UQ analysis is to estimate the probabilistic characteristics of an output random variable $Y = y(\mathbf{X})$, including its statistical moments and CDF, when the probability law of the input random vector \mathbf{X} is prescribed. More often than not, Y is assumed to belong to a reasonably large class of random variables, such as the weighted L^2 space

$$L^2(\Omega, \mathcal{F}, \mathbb{P}) := \left\{ Y : \Omega \rightarrow \mathbb{R} : \int_{\Omega} |y(\mathbf{X}(\omega))|^2 d\mathbb{P}(\omega) = \int_{\mathbb{A}^N} |y(\mathbf{x})|^2 f_{\mathbf{X}}(\mathbf{x}) d\mathbf{x} < \infty \right\}, \tag{13}$$

which is a Hilbert space with the inner product

$$(y(\mathbf{X}), z(\mathbf{X}))_{L^2(\Omega, \mathcal{F}, \mathbb{P})} := \int_{\Omega} y(\mathbf{X}(\omega))z(\mathbf{X}(\omega)) d\mathbb{P}(\omega) = \int_{\mathbb{A}^N} y(\mathbf{x})z(\mathbf{x})f_{\mathbf{X}}(\mathbf{x}) d\mathbf{x} \tag{14}$$

and norm

$$\|y(\mathbf{X})\|_{L^2(\Omega, \mathcal{F}, \mathbb{P})} := \sqrt{(y(\mathbf{X}), y(\mathbf{X}))_{L^2(\Omega, \mathcal{F}, \mathbb{P})}} = \sqrt{\int_{\Omega} y^2(\mathbf{X}(\omega)) d\mathbb{P}(\omega)} = \sqrt{\int_{\mathbb{A}^N} y^2(\mathbf{x})f_{\mathbf{X}}(\mathbf{x}) d\mathbf{x}}. \tag{15}$$

4. Univariate basis functions

Let $\mathbf{x} = (x_1, \dots, x_N)$ be an arbitrary point in \mathbb{A}^N . For the coordinate direction k , $k = 1, \dots, N$, define a non-negative integer $p_k \in \mathbb{N}_0$ and a positive integer $n_k \geq p_k + 1$, representing the degree or order² and total number of basis functions, respectively. The rest of this section briefly describes necessary details of univariate B-splines.

² Degree and order are used interchangeably in this paper.

4.1. Standard B-splines

For the coordinate direction $k = 1, \dots, N$, define a knot vector

$$\xi_k := \{\xi_{k,i_k}\}_{i_k=1}^{n_k+p_k+1} = \{a_k = \xi_{k,1}, \xi_{k,2}, \dots, \xi_{k,n_k+p_k+1} = b_k\} \tag{16}$$

on the interval $[a_k, b_k]$ by a non-decreasing sequence of real numbers, where ξ_{k,i_k} is the i_k th knot with $i_k = 1, 2, \dots, n_k + p_k + 1$. Any knot may appear up to $p_k + 1$ times in the sequence. Hence, the knot vector can be rewritten as

$$\xi_k = \{a_k = \underbrace{\zeta_{k,1}, \dots, \zeta_{k,1}}_{m_{k,1} \text{ times}}, \underbrace{\zeta_{k,2}, \dots, \zeta_{k,2}}_{m_{k,2} \text{ times}}, \dots, \underbrace{\zeta_{k,r_k-1}, \dots, \zeta_{k,r_k-1}}_{m_{k,r_k-1} \text{ times}}, \underbrace{\zeta_{k,r_k}, \dots, \zeta_{k,r_k}}_{m_{k,r_k} \text{ times}} = b_k\}, \tag{17}$$

$$a_k = \zeta_{k,1} < \zeta_{k,2} < \dots < \zeta_{k,r_k-1} < \zeta_{k,r_k} = b_k,$$

where ζ_{k,j_k} , $j_k = 1, 2, \dots, r_k$, are r_k unique knots, each of which has multiplicity $1 \leq m_{k,j_k} \leq p_k + 1$. A knot vector is called $(p_k + 1)$ -open if the end knots have multiplicities $p_k + 1$. In this work, only $(p_k + 1)$ -open knot vectors are considered. For more details, readers are referred to [Appendix](#) of this paper and Chapter 2 of the book by Cottrell et al. [35].

Denote by $B_{i_k,p_k,\xi_k}^k(x_k)$ the i_k th univariate B-spline with degree p_k . Given the knot vector ξ_k and zero-degree basis functions, all higher-order B-spline functions on $[a_k, b_k]$ are defined recursively, where $1 \leq k \leq N$, $1 \leq i_k \leq n_k$, and $1 \leq p_k < \infty$. See [Appendix](#) for an explicit definition of $B_{i_k,p_k,\xi_k}^k(x_k)$.

The B-splines are bequeathed with a number of attractive properties, delivering superb approximating power to numerical methods. More precisely, they are [35,36]: (1) non-negative; (2) locally supported on the interval $[\xi_{k,i_k}, \xi_{k,i_k+p_k+1})$ for all i_k ; (3) linearly independent; (4) committed to partition of unity; and (5) pointwise C^∞ -continuous everywhere except at the knots ζ_{k,j_k} of multiplicity m_{k,j_k} for all j_k , where they are $C^{p_k-m_{k,j_k}}$ -continuous, provided that $1 \leq m_{k,j_k} < p_k + 1$.

4.2. Measure-consistent orthonormalized B-splines

The aforementioned B-splines, although they form a basis of the spline space of degree p_k and knot vector ξ_k , are not necessarily orthogonal with respect to the probability measure $f_{X_k}(x_k) dx_k$ of X_k . A three-step procedure, originally proposed in a past work [32], is summarized here to generate their orthonormal version.

- (1) Given a set of B-splines of degree p_k , create an auxiliary set by replacing any element, arbitrarily chosen to be the first, with one. Arrange the elements of the set into an n_k -dimensional vector

$$\mathbf{P}_k(x_k) := \left(1, B_{2,p_k,\xi_k}^k(x_k), \dots, B_{n_k,p_k,\xi_k}^k(x_k)\right)^T \tag{18}$$

comprising the auxiliary B-splines. The linear independence of the auxiliary B-splines is preserved [32].

- (2) Construct an $n_k \times n_k$ spline moment matrix

$$\mathbf{G}_k := \mathbb{E}[\mathbf{P}_k(X_k)\mathbf{P}_k^T(X_k)]. \tag{19}$$

The matrix \mathbf{G}_k exists because X_k has finite moments up to order $2p_k$, as stated in [Assumption 1](#). Furthermore, it is symmetric and positive-definite [32], ensuring the existence of a non-singular $n_k \times n_k$ whitening matrix \mathbf{W}_k such that

$$\mathbf{W}_k^T \mathbf{W}_k = \mathbf{G}_k^{-1}. \tag{20}$$

- (3) Apply a whitening transformation to create a vector of orthonormalized B-splines

$$\boldsymbol{\psi}_k(x_k) = \mathbf{W}_k \mathbf{P}_k(x_k), \tag{21}$$

consisting of uncorrelated components

$$\psi_{i_k,p_k,\xi_k}^k(x_k), \quad i_k = 1, \dots, n_k, \quad k = 1, \dots, N.$$

Note that the invertibility of \mathbf{G}_k does not uniquely determine \mathbf{W}_k . Indeed, there are several ways to choose \mathbf{W}_k such that the condition described in Step (2) is satisfied [32]. One prominent, relatively stable option is to invoke the Cholesky factorization $\mathbf{G}_k = \mathbf{Q}_k \mathbf{Q}_k^T$, leading to

$$\mathbf{W}_k = \mathbf{Q}_k^{-1}, \tag{22}$$

where \mathbf{Q}_k is an $n_k \times n_k$ lower-triangular matrix. As a result, the transformation becomes

$$\boldsymbol{\psi}_k(x_k) = \mathbf{Q}_k^{-1} \mathbf{P}_k(x_k), \tag{23}$$

where the orthonormal splines are obtained by linear combinations of auxiliary B-splines. The rest of the paper will use the Cholesky factorization.

5. Orthogonal spline expansions

In this section, two novel UQ methods exploiting measure-consistent B-splines are presented for solving both classes of UQ problems discussed in Section 3. The methods are founded on Fourier-spline expansion of any square-integrable output function of interest.

5.1. Spline chaos expansion

The input random vector \mathbf{X} , as it subsumes independent components, is endowed with a product-type probability measure. Therefore, multivariate orthonormalized B-splines in N variables are readily constructed from an N -dimensional tensor product of univariate orthonormalized B-splines, resulting in SCE.

5.1.1. Multivariate orthonormalized basis

Define three multi-indices $\mathbf{i} := (i_1, \dots, i_N) \in \mathbb{N}^N$, $\mathbf{n} := (n_1, \dots, n_N) \in \mathbb{N}^N$, and $\mathbf{p} := (p_1, \dots, p_N) \in \mathbb{N}_0^N$, representing the knot indices, numbers of basis functions, and degrees of splines, respectively, in all N coordinate directions. Denote by $\Xi := \{\xi_1, \dots, \xi_N\}$ a family of all N knot vectors. Associated with \mathbf{i} , define an index set

$$I_{\mathbf{n}} := \{\mathbf{i} = (i_1, \dots, i_N) : 1 \leq i_k \leq n_k, k = 1, \dots, N\} \subset \mathbb{N}^N \quad (24)$$

with cardinality

$$|I_{\mathbf{n}}| = \prod_{k=1}^N n_k. \quad (25)$$

For the coordinate direction k , define by

$$I_k := r_k - 1 \quad (26)$$

the number of subintervals corresponding to the knot vector ξ_k with r_k distinct knots. Then the partition defined by the knot sequences ξ_k , $k = 1, \dots, N$, splits $\mathbb{A}^N := \times_{k=1}^N [a_k, b_k]$ into smaller N -dimensional rectangles

$$\left\{ \mathbf{x} = (x_1, \dots, x_N) : \zeta_{k,j_k} \leq x_k < \zeta_{k,j_k+1}, k = 1, \dots, N \right\}, j_k = 1, \dots, I_k, \quad (27)$$

where ζ_{k,j_k} is the j_k th distinct knot in the coordinate direction k . A mesh is defined by a partition of \mathbb{A}^N into such rectangular elements. Define the largest element size in each coordinate direction k by

$$h_k := \max_{j_k=1, \dots, I_k} (\zeta_{k,j_k+1} - \zeta_{k,j_k}), k = 1, \dots, N. \quad (28)$$

Then, given the family of knot sequences $\Xi = \{\xi_1, \dots, \xi_N\}$,

$$\mathbf{h} := (h_1, \dots, h_N) \text{ and } h := \max_{k=1, \dots, N} h_k \quad (29)$$

define a vector of the largest element sizes in all N coordinates and the global element size, respectively, for the domain \mathbb{A}^N . As a result, the multivariate orthonormalized B-splines in \mathbf{x} consistent with the probability measure $f_{\mathbf{X}}(\mathbf{x})d\mathbf{x}$ are obtained from the product

$$\Psi_{\mathbf{i}, \mathbf{p}, \Xi}(\mathbf{x}) := \prod_{k=1}^N \psi_{i_k, p_k, \xi_k}^k(x_k), \quad \mathbf{i} = (i_1, \dots, i_N) \in I_{\mathbf{n}}. \quad (30)$$

When the input random variables X_1, \dots, X_N , instead of real variables x_1, \dots, x_N , are inserted in the argument, the multivariate splines $\Psi_{\mathbf{i}, \mathbf{p}, \Xi}(\mathbf{X})$, $\mathbf{i} \in I_{\mathbf{n}}$, become functions of input random variables. Their second-moment properties are [32]

$$\mathbb{E} [\Psi_{\mathbf{i}, \mathbf{p}, \Xi}(\mathbf{X})] = \begin{cases} 1, & \mathbf{i} = \mathbf{1} := (1, \dots, 1), \\ 0, & \mathbf{i} \neq \mathbf{1}, \end{cases} \quad (31)$$

and

$$\mathbb{E} [\Psi_{\mathbf{i}, \mathbf{p}, \Xi}(\mathbf{X}) \Psi_{\mathbf{j}, \mathbf{p}, \Xi}(\mathbf{X})] = \begin{cases} 1, & \mathbf{i} = \mathbf{j}, \\ 0, & \mathbf{i} \neq \mathbf{j}. \end{cases} \quad (32)$$

5.1.2. SCE approximation

Given a degree \mathbf{p} and a family of knot sequences Ξ , recall that $\{\Psi_{\mathbf{i}, \mathbf{p}, \Xi}(\mathbf{X}) : \mathbf{i} \in I_{\mathbf{n}}\}$ represents the set comprising multivariate orthonormalized B-splines that is consistent with the probability measure $f_{\mathbf{X}}(\mathbf{x})d\mathbf{x}$. Then, for any random variable $y(\mathbf{X}) \in L^2(\Omega, \mathcal{F}, \mathbb{P})$, there exists an orthogonal expansion in multivariate orthonormal splines in \mathbf{X} , referred to as an SCE approximation [32]

$$y_{\mathbf{p}, \Xi}(\mathbf{X}) := \sum_{\mathbf{i} \in I_{\mathbf{n}}} C_{\mathbf{i}, \mathbf{p}, \Xi} \Psi_{\mathbf{i}, \mathbf{p}, \Xi}(\mathbf{X}) \quad (33)$$

of $y(\mathbf{X})$, where the SCE expansion coefficients $C_{\mathbf{i}, \mathbf{p}, \Xi} \in \mathbb{R}$, $\mathbf{i} \in \mathcal{I}_n$, are defined as

$$C_{\mathbf{i}, \mathbf{p}, \Xi} := \mathbb{E} [y(\mathbf{X})\Psi_{\mathbf{i}, \mathbf{p}, \Xi}(\mathbf{X})] := \int_{\mathbb{A}^N} y(\mathbf{x})\Psi_{\mathbf{i}, \mathbf{p}, \Xi}(\mathbf{x})f_{\mathbf{X}}(\mathbf{x})d\mathbf{x}, \quad \mathbf{i} \in \mathcal{I}_n. \tag{34}$$

According to Eq. (33), the SCE of any random variable $y(\mathbf{X}) \in L^2(\Omega, \mathcal{F}, \mathbb{P})$ is an orthogonal projection onto the spline space $S_{\mathbf{p}, \Xi}$ (say) spanning the set of measure-consistent multivariate orthonormalized B-splines.

5.2. Spline dimensional decomposition

Due to the tensor-product structure, the number of basis functions of SCE escalates rapidly when confronted with high-dimensional UQ problems. Therefore, development of an alternative expansion, referred to as SDD, which is capable of exploiting low effective dimensions [37] of high-dimensional functions, is desirable.

5.2.1. Dimensionwise multivariate orthonormal basis

Denote by $\emptyset \neq u = \{k_1, \dots, k_{|u|}\} \subseteq \{1, \dots, N\}$ a non-empty subset of the index set $\{1, \dots, N\}$ with cardinality $1 \leq |u| \leq N$. For such a subset, let $\mathbf{X}_u := (X_{k_1}, \dots, X_{k_{|u|}})^T$ be a subvector of \mathbf{X} defined on the abstract probability space $(\Omega^u, \mathcal{F}^u, \mathbb{P}^u)$, where Ω^u is the sample space of \mathbf{X}_u , \mathcal{F}^u is a σ -algebra on Ω^u , and \mathbb{P}^u is a probability measure. As \mathbf{X} comprises independent random variables, the PDF of \mathbf{X}_u is

$$f_{\mathbf{X}_u}(\mathbf{x}_u) = \prod_{k \in u} f_{X_k}(x_k) = \prod_{l=1}^{|u|} f_{X_{k_l}}(x_{k_l}), \quad \mathbf{x}_u := (x_{k_1}, \dots, x_{k_{|u|}})^T. \tag{35}$$

Define three multi-indices $\mathbf{i}_u := (i_{k_1}, \dots, i_{k_{|u|}}) \in \mathbb{N}^{|u|}$, $\mathbf{n}_u := (n_{k_1}, \dots, n_{k_{|u|}}) \in \mathbb{N}^{|u|}$, and $\mathbf{p}_u := (p_{k_1}, \dots, p_{k_{|u|}}) \in \mathbb{N}_0^{|u|}$, representing the knot indices, numbers of basis functions, and degrees of splines, respectively, in all $|u|$ coordinate directions. Denote by $\Xi_u := \{\xi_{k_1}, \dots, \xi_{k_{|u|}}\}$ a family of all $|u|$ knot sequences. Associated with \mathbf{i}_u , define an index set

$$\mathcal{I}_{u, \mathbf{n}_u} := \left\{ \mathbf{i}_u = (i_{k_1}, \dots, i_{k_{|u|}}) : 1 \leq i_{k_l} \leq n_{k_l}, l = 1, \dots, |u| \right\} \subset \mathbb{N}^{|u|} \tag{36}$$

with cardinality

$$|\mathcal{I}_{u, \mathbf{n}_u}| = \prod_{k \in u} n_k. \tag{37}$$

For the coordinate direction k_l , define by

$$I_{k_l} := r_{k_l} - 1 \tag{38}$$

the number of subintervals corresponding to the knot vector ξ_{k_l} with r_{k_l} distinct knots. Then the partition, defined by the knot vectors $\xi_{k_1}, \dots, \xi_{k_{|u|}}$, decomposes the $|u|$ -dimensional rectangle $\mathbb{A}^u := \times_{k \in u} [a_k, b_k]$ into smaller rectangles

$$\left\{ \mathbf{x}_u = (x_{k_1}, \dots, x_{k_{|u|}}) : \zeta_{k_l, j_{k_l}} \leq x_{k_l} < \zeta_{k_l, j_{k_l}+1}, l = 1, \dots, |u| \right\}, \quad j_{k_l} = 1, \dots, I_{k_l}, \tag{39}$$

where $\zeta_{k_l, j_{k_l}}$ is the j_{k_l} th distinct knot in the coordinate direction k_l . A mesh is defined by a partition of \mathbb{A}^u into such rectangular elements. Define the largest element size in each coordinate direction $k \in u$ by

$$h_{u, k_l} := \max_{j_{k_l}=1, \dots, I_{k_l}} (\zeta_{k_l, j_{k_l}+1} - \zeta_{k_l, j_{k_l}}), \quad l = 1, \dots, |u|. \tag{40}$$

Then, given the knot vectors $\Xi_u = \{\xi_{k_1}, \dots, \xi_{k_{|u|}}\}$,

$$\mathbf{h}_u := (h_{u, k_1}, \dots, h_{u, k_{|u|}}) \quad \text{and} \quad h_u := \max_{l=1, \dots, |u|} h_{u, k_l} \tag{41}$$

define a vector of the largest element sizes in all $|u|$ coordinates and the global mesh size, respectively, for the domain \mathbb{A}^u . Consequently, for $\emptyset \neq u = \{k_1, \dots, k_{|u|}\} \subseteq \{1, \dots, N\}$, with $\mathbf{p}_u = (p_{k_1}, \dots, p_{k_{|u|}}) \in \mathbb{N}_0^{|u|}$ and $\Xi_u = \{\xi_{k_1}, \dots, \xi_{k_{|u|}}\}$ in mind, the multivariate orthonormalized B-splines in $\mathbf{x}_u = (x_{k_1}, \dots, x_{k_{|u|}})$ consistent with the probability measure $f_{\mathbf{X}_u}(\mathbf{x}_u) d\mathbf{x}_u$ are

$$\Psi_{\mathbf{i}_u, \mathbf{p}_u, \Xi_u}^u(\mathbf{x}_u) = \prod_{k \in u} \psi_{i_k, p_k, \xi_k}^k(x_k) = \prod_{l=1}^{|u|} \psi_{i_{k_l}, p_{k_l}, \xi_{k_l}}^{k_l}(x_{k_l}), \quad \mathbf{i}_u = (i_{k_1}, \dots, i_{k_{|u|}}) \in \bar{\mathcal{I}}_{u, \mathbf{n}_u}, \tag{42}$$

where

$$\bar{\mathcal{I}}_{u, \mathbf{n}_u} := \left\{ \mathbf{i}_u = (i_{k_1}, \dots, i_{k_{|u|}}) : 2 \leq i_{k_l} \leq n_{k_l}, l = 1, \dots, |u| \right\} \subset (\mathbb{N} \setminus \{1\})^{|u|} \tag{43}$$

is a reduced index set, which has cardinality

$$|\bar{\mathcal{I}}_{u, \mathbf{n}_u}| := \prod_{k \in u} (n_k - 1). \tag{44}$$

The key difference between the index sets \bar{I}_{u,n_u} and I_{u,n_u} is that the former limits the range of index i_{k_l} , $l = 1, \dots, |u|$, associated with the k_l th variable x_{k_l} , to $2, \dots, n_{k_l}$. The exclusion of $i_{k_l} = 1$ removes the first constant element of $\Psi_{k_l}(x_{k_l})$ in order to prevent reduction of the degree of interaction of the corresponding multivariate spline basis below $|u|$.

When the input random variables X_1, \dots, X_N , instead of real variables x_1, \dots, x_N , are inserted in the argument, the multivariate splines $\Psi_{\mathbf{i}_u, \mathbf{p}_u, \Xi_u}^u(\mathbf{X}_u)$, $\emptyset \neq u \subseteq \{1, \dots, N\}$, $\mathbf{i}_u \in \bar{I}_{u,n_u}$, become functions of random input variables. Then, for $\emptyset \neq u, v \subseteq \{1, \dots, N\}$, $\mathbf{i}_u \in \bar{I}_{u,n_u}$, and $\mathbf{j}_v \in \bar{I}_{v,n_v}$, the first- and second-order moments of multivariate orthonormalized B-splines are [33]

$$\mathbb{E} \left[\Psi_{\mathbf{i}_u, \mathbf{p}_u, \Xi_u}^u(\mathbf{X}_u) \right] = 0 \tag{45}$$

and

$$\mathbb{E} \left[\Psi_{\mathbf{i}_u, \mathbf{p}_u, \Xi_u}^u(\mathbf{X}_u) \Psi_{\mathbf{j}_v, \mathbf{p}_v, \Xi_v}^v(\mathbf{X}_v) \right] = \begin{cases} 1, & u = v \text{ and } \mathbf{i}_u = \mathbf{j}_v, \\ 0, & \text{otherwise,} \end{cases} \tag{46}$$

respectively.

5.2.2. SDD approximation

Suppose the degree and family of knot sequences in all coordinate directions have been specified as $\mathbf{p} = (p_1, \dots, p_N) \in \mathbb{N}_0^{N|}$ and $\Xi = \{\xi_1, \dots, \xi_N\}$, respectively. For $\emptyset \neq u \subseteq \{1, \dots, N\}$ and $\mathbf{X}_u := (X_{k_1}, \dots, X_{k_{|u|}})^T : (\Omega^u, \mathcal{F}^u) \rightarrow (\mathbb{A}^u, \mathcal{B}^u)$, with $\mathbf{p}_u = (p_{k_1}, \dots, p_{k_{|u|}}) \in \mathbb{N}_0^{|u|}$ and $\Xi_u = \{\xi_{k_1}, \dots, \xi_{k_{|u|}}\}$ in mind, denote by $\{\Psi_{\mathbf{i}_u, \mathbf{p}_u, \Xi_u}^u(\mathbf{X}_u) : \mathbf{i}_u \in \bar{I}_{u,n_u}\}$ a set comprising multivariate orthonormalized B-splines that is consistent with the probability measure $f_{\mathbf{X}_u}(\mathbf{x}_u) d\mathbf{x}_u$. Then, for any random variable $y(\mathbf{X}) \in L^2(\Omega, \mathcal{F}, \mathbb{P})$, there exists a hierarchically expanded Fourier-like series in multivariate orthonormal splines in \mathbf{X}_u , referred to as the SDD [33]

$$y_{\mathbf{p}, \Xi}(\mathbf{X}) := y_{\emptyset} + \sum_{\emptyset \neq u \subseteq \{1, \dots, N\}} \sum_{\mathbf{i}_u \in \bar{I}_{u,n_u}} C_{\mathbf{i}_u, \mathbf{p}_u, \Xi_u}^u \Psi_{\mathbf{i}_u, \mathbf{p}_u, \Xi_u}^u(\mathbf{X}_u) \tag{47}$$

of $y(\mathbf{X})$, where the SDD expansion coefficients $y_{\emptyset} \in \mathbb{R}$ and $C_{\mathbf{i}_u, \mathbf{p}_u, \Xi_u}^u \in \mathbb{R}$, $\emptyset \neq u \subseteq \{1, \dots, N\}$, $\mathbf{i}_u \in \bar{I}_{u,n_u}$, are defined as

$$y_{\emptyset} := \mathbb{E} [y(\mathbf{X})] := \int_{\mathbb{A}^N} y(\mathbf{x}) f_{\mathbf{X}}(\mathbf{x}) d\mathbf{x}, \tag{48}$$

$$C_{\mathbf{i}_u, \mathbf{p}_u, \Xi_u}^u := \mathbb{E} \left[y(\mathbf{X}) \Psi_{\mathbf{i}_u, \mathbf{p}_u, \Xi_u}^u(\mathbf{X}_u) \right] := \int_{\mathbb{A}^N} y(\mathbf{x}) \Psi_{\mathbf{i}_u, \mathbf{p}_u, \Xi_u}^u(\mathbf{x}_u) f_{\mathbf{X}}(\mathbf{x}) d\mathbf{x}, \quad \mathbf{i}_u \in \bar{I}_{u,n_u}. \tag{49}$$

In a practical setting, the output function $y(\mathbf{X})$ is likely to have an effective dimension [37] much lower than N , meaning that the right side of Eq. (47) can be effectively approximated by a sum of lower-dimensional component functions of $y_{\mathbf{p}, \Xi}(\mathbf{X})$ but still maintain all random variables \mathbf{X} of a high-dimensional UQ problem. Due to the dimensional hierarchical structure of SDD, this can be done keeping all basis functions in at most $1 \leq S \leq N$ variables, thereby retaining the degrees of interaction among input variables less than or equal to S . The result is an S -variate SDD approximation

$$y_{S, \mathbf{p}, \Xi}(\mathbf{X}) := y_{\emptyset} + \sum_{\substack{\emptyset \neq u \subseteq \{1, \dots, N\} \\ 1 \leq |u| \leq S}} \sum_{\mathbf{i}_u \in \bar{I}_{u,n_u}} C_{\mathbf{i}_u, \mathbf{p}_u, \Xi_u}^u \Psi_{\mathbf{i}_u, \mathbf{p}_u, \Xi_u}^u(\mathbf{X}_u) \tag{50}$$

of $y(\mathbf{X})$. When $S \ll N$, as it is anticipated to hold in real-life applications, the number of coefficients in the SDD approximation drops precipitously, ushering in substantial savings of computational effort.

When $S = 1$ or $S = 2$, the resulting SDD approximations are referred to as univariate and bivariate SDD approximations, respectively. In such cases, the functions $y_{1, \mathbf{p}, \Xi}(\mathbf{X})$ or $y_{2, \mathbf{p}, \Xi}(\mathbf{X})$ should not be interpreted as first- and second-order approximations, as S does not limit the accuracy of SDD in capturing the potential nonlinearity of $y(\mathbf{X})$. On the contrary, depending on how the orders and knot vectors are chosen, arbitrarily high-order univariate and bivariate terms of $y(\mathbf{X})$, including discontinuity and nonsmoothness, could be lurking inside $y_{1, \mathbf{p}, \Xi}(\mathbf{X})$ or $y_{2, \mathbf{p}, \Xi}(\mathbf{X})$.

5.3. Computational cost

The computational cost and complexity of SCE and SDD approximations with respect to stochastic dimension N can be judged by examining the corresponding numbers of basis functions involved. To do so, consider the SCE approximation in Eq. (33) and the S -variate SDD approximation in Eq. (50). The numbers of basis functions from such SCE and SDD approximations are

$$L_{\mathbf{p}, \Xi} = \prod_{k=1}^N n_k \tag{51}$$

and

$$L_{S, \mathbf{p}, \Xi} = 1 + \sum_{\substack{\emptyset \neq u \subseteq \{1, \dots, N\} \\ 1 \leq |u| \leq S}} \prod_{k \in u} (n_k - 1) \leq \prod_{k=1}^N n_k = L_{\mathbf{p}, \Xi}, \tag{52}$$

respectively. If $n_k = n$ for all $k = 1, \dots, N$, then $L_{\mathbf{p}, \Xi} = \mathcal{O}(n^N)$ from Eq. (51) and $L_{S, \mathbf{p}, \Xi} = \mathcal{O}(n^S N^S)$ from Eq. (52). Hence, given a fixed value of n , the computational effort with respect to N grows exponentially for the SCE approximation and S -degree polynomially

for the SDD approximation. For example, when $N = 10$ and $n = 5$, the univariate ($S = 1$) and bivariate ($S = 2$) SDD approximations involve 41 and 761 basis functions, respectively. In contrast, the number of basis functions in the SCE approximation jumps to 5^{10} , which is significantly greater than that required by either of the two SDD approximations. Therefore, SDD reduces the curse of dimensionality of SCE by a substantial extent. Having said this, SCE is still useful for fundamental studies on low-dimensional academic-type problems, while SDD, due to its improved scalability, is meant for tackling high-dimensional practical problems expected in real-life applications. Numerical examples featuring SCE and SDD will be presented in a forthcoming section.

5.4. Convergence

For any $y(\mathbf{X}) \in L^2(\Omega, \mathcal{F}, \mathbb{P})$, a sequence of SCE approximations $\{y_{\mathbf{p},\varepsilon}(\mathbf{X})\}_{\mathbf{h}>\mathbf{0}}$, with $\mathbf{h} = (h_1, \dots, h_N)$ representing the vector of largest element sizes, converges to $y(\mathbf{X})$ in mean-square [32], that is,

$$\lim_{\mathbf{h} \rightarrow \mathbf{0}} \mathbb{E} \left[\left| y(\mathbf{X}) - y_{\mathbf{p},\varepsilon}(\mathbf{X}) \right|^2 \right] = 0. \tag{53}$$

In addition, if $S = N$, then $y_{N,\mathbf{p},\varepsilon}(\mathbf{X}) = y_{\mathbf{p},\varepsilon}(\mathbf{X})$. Therefore, the sequence of SDD approximations $\{y_{S,\mathbf{p},\varepsilon}(\mathbf{X})\}_{1 \leq S \leq N, \mathbf{h}>\mathbf{0}}$ also converges to $y(\mathbf{X})$ in mean-square [33], that is,

$$\lim_{S \rightarrow N, \mathbf{h} \rightarrow \mathbf{0}} \mathbb{E} \left[\left| y(\mathbf{X}) - y_{S,\mathbf{p},\varepsilon}(\mathbf{X}) \right|^2 \right] = 0. \tag{54}$$

Moreover, as the SCE and SDD approximations both converge in mean-square, they also converge in probability and in distribution. Readers interested in formal proofs are directed to prior theoretical works [32,33].

5.5. Output statistics and other properties

The SCE and SDD approximations $y_{\mathbf{p},\varepsilon}(\mathbf{X})$ and $y_{S,\mathbf{p},\varepsilon}(\mathbf{X})$ can both be viewed as surrogates of $y(\mathbf{X})$. Therefore, relevant probabilistic characteristics of $y(\mathbf{X})$, including its first two moments and PDF, if it exists, can be estimated from the statistical properties of these approximations.

Applying the expectation operator on $y_{\mathbf{p},\varepsilon}(\mathbf{X})$ in Eq. (33) and $y_{S,\mathbf{p},\varepsilon}(\mathbf{X})$ in Eq. (50) and recognizing Eqs. (31) and (45), the means of SCE and SDD approximations

$$\mathbb{E} [y_{\mathbf{p},\varepsilon}(\mathbf{X})] = \mathbb{E} [y_{S,\mathbf{p},\varepsilon}(\mathbf{X})] = C_{\mathbf{1},\mathbf{p},\varepsilon} = y_\theta = \mathbb{E} [y(\mathbf{X})], \quad \mathbf{1} = (1, \dots, 1), \tag{55}$$

are the same and independent of S , \mathbf{p} , and ε . More importantly, the SCE and SDD approximations always yield the exact mean, provided that the expansion coefficient $C_{\mathbf{1},\mathbf{p},\varepsilon}$ or y_θ is determined exactly.

Applying the expectation operator on $[y_{\mathbf{p},\varepsilon}(\mathbf{X}) - C_{\mathbf{1},\mathbf{p},\varepsilon}]^2$ and $[y_{S,\mathbf{p},\varepsilon}(\mathbf{X}) - y_\theta]^2$ and employing Eqs. (31), (32), (45), and (46) results in the variance

$$\text{var} [y_{\mathbf{p},\varepsilon}(\mathbf{X})] = \sum_{i \in \mathcal{I}_n} C_{i,\mathbf{p},\varepsilon}^2 - C_{\mathbf{1},\mathbf{p},\varepsilon}^2 \leq \text{var} [y(\mathbf{X})] \tag{56}$$

of $y_{\mathbf{p},\varepsilon}(\mathbf{X})$ and in the variance

$$\text{var} [y_{S,\mathbf{p},\varepsilon}(\mathbf{X})] = \sum_{\substack{\emptyset \neq u \subseteq \{1, \dots, N\} \\ 1 \leq |u| \leq S}} \sum_{i_u \in \mathcal{I}_{u,\mathbf{p}_u}} \left(C_{i_u,\mathbf{p}_u,\varepsilon_u}^u \right)^2 \leq \text{var} [y(\mathbf{X})] \tag{57}$$

of $y_{S,\mathbf{p},\varepsilon}(\mathbf{X})$. Therefore, the second-moment properties of SCE/SDD approximations are solely determined by the relevant expansion coefficients. The formulae for the mean and variance of the SCE/SDD approximations are the same as those reported for the PCE/PDD approximations [3,5], although the respective expansion coefficients involved are not. The primary reason for this similarity is rooted in the use of the orthonormal basis in both expansions.

Being convergent in probability and in distribution, the PDF and CDF of $y(\mathbf{X})$, if they exist, can also be estimated economically by resampling $y_{\mathbf{p},\varepsilon}(\mathbf{X})$ or $y_{S,\mathbf{p},\varepsilon}(\mathbf{X})$. They will be illustrated in numerical examples.

5.6. A few remarks

From the independence of input random variables stated in Assumption 1, the stochastic domain \mathbb{A}^N is always a rectangle. Therefore, B-splines are appropriate or adequate for function approximations on that domain. If the domain is non-rectangular, such as those expected for dependent random variables, then more advanced non-uniform rational basis splines (NURBS) or T-splines may be considered. However, tackling dependent random variables head-on is not a trivial task in general, because multivariate basis functions can no longer be constructed from the tensorization of univariate basis functions. Having said so, the use of NURBS or T-spline becomes necessary for function approximations on physical domains with boundary described by free-form surfaces and conic sections, such as circles, ellipses, cylinders, spheres, ellipsoids, and tori. In this case, NURBS functions equipped with judiciously selected weights can represent the physical domain exactly [35]. This was exemplified in the authors' recent work on stochastic isogeometric analysis where NURBS are used for describing geometry, displacement responses, and random field discretization, but B-splines are still used for stochastic analysis [38]. It is worth mentioning that a deterministic meta modeling technique using NURBS

in tandem with an optimization strategy has been reported to ascertain the NURBS parameters automatically [39]. Additionally, there exists an enhanced version of SDD where the knot vectors have been derived optimally [40].

The orthonormalized B-splines in SCE and SDD are both consistent with arbitrary probability measures of input random variables with bounded domains. However, there are many UQ problems where there exist random variables with unbounded domains. In such a case, an appropriate probability preserving transformation, mapping a random variable with unbounded domain to another with bounded domain is required. The transformation will be identified when numerical examples are presented.

6. Calculation of expansion coefficients

A natural propensity for calculating the SCE and SDD coefficients is to invoke their respective definitions in Eqs. (34), (48), and (49), followed by numerical integration. However, in practical applications, the output function y is often determined algorithmically by performing time-consuming FEA or other expensive numerical calculations. Clearly, for a high-dimensional UQ problem, say, with N exceeding ten, evaluating the N -dimensional sums stemming from an N -dimensional numerical integration is computationally formidable and likely prohibitive. While reduced-order methods, such as the dimension-reduction techniques [38,41], have been used to curb the computational demand by a great magnitude, here, a more practical alternative to numerical integration, such as regression analysis, is exploited to estimate these coefficients.

6.1. SCE and SDD approximations: single-index versions

For a simpler description of SCE/SDD approximations, consider listing the terms of the expansions with respect to a single index. In reference to the concise forms of SCE in (33) and SDD in (50), arrange the elements of the sets

$$\left\{ \Psi_{\mathbf{i}, \mathbf{p}, \Xi}(\mathbf{X}) : \mathbf{i} \in I_{n_u} \right\} = \left\{ \phi_1(\mathbf{X}), \dots, \phi_{L_{\mathbf{p}, \Xi}}(\mathbf{X}) \right\} \tag{58}$$

and

$$\left\{ \Psi_{\mathbf{i}_u, \mathbf{p}_u, \Xi_u}^u(\mathbf{X}_u) : 1 \leq |u| \leq S, \mathbf{i}_u \in \bar{I}_{u, n_u} \right\} = \left\{ \varphi_2(\mathbf{X}), \dots, \varphi_{L_{S, \mathbf{p}, \Xi}}(\mathbf{X}) \right\}, \quad \varphi_1(\mathbf{X}) = 1, \tag{59}$$

consisting of $L_{\mathbf{p}, \Xi}$ and $L_{S, \mathbf{p}, \Xi}$ basis functions, respectively. By doing so, the same basis functions of SCE and SDD in the sets are indexed with a single integer i . Obviously, the basis functions $\phi_i(\mathbf{X})$ and $\varphi_i(\mathbf{X})$ also depend on \mathbf{p} and Ξ , but the latter symbols are suppressed for brevity.

Associated with each $i = 1, \dots, L_{\mathbf{p}, \Xi}$ or $i = 1, \dots, L_{S, \mathbf{p}, \Xi}$, denote by $C_i \in \mathbb{R}$ or $\bar{C}_i \in \mathbb{R}$ the i th SCE or SDD coefficient. As a result, the SCE and S -variate SDD approximations can also be written as

$$y_{\mathbf{p}, \Xi}(\mathbf{X}) := \sum_{i=1}^{L_{\mathbf{p}, \Xi}} C_i \phi_i(\mathbf{X}), \quad C_i := \int_{\mathbb{A}^N} y(\mathbf{x}) \phi_i(\mathbf{X}) f_{\mathbf{X}}(\mathbf{x}) \, d\mathbf{x}, \quad i = 1, \dots, L_{\mathbf{p}, \Xi}. \tag{60}$$

and

$$y_{S, \mathbf{p}, \Xi}(\mathbf{X}) := \sum_{i=1}^{L_{S, \mathbf{p}, \Xi}} \bar{C}_i \varphi_i(\mathbf{X}), \quad \bar{C}_i := \int_{\mathbb{A}^N} y(\mathbf{x}) \varphi_i(\mathbf{X}) f_{\mathbf{X}}(\mathbf{x}) \, d\mathbf{x}, \quad i = 1, \dots, L_{S, \mathbf{p}, \Xi}, \tag{61}$$

respectively.

Henceforth, the mean and variances of $y_{\mathbf{p}, \Xi}(\mathbf{X})$ and $y_{S, \mathbf{p}, \Xi}(\mathbf{X})$ are calculated from the expansion coefficients as

$$\mathbb{E} [y_{\mathbf{p}, \Xi}(\mathbf{X})] = \mathbb{E} [y_{S, \mathbf{p}, \Xi}(\mathbf{X})] = C_1 = \bar{C}_1 = \mathbb{E} [y(\mathbf{X})] \tag{62}$$

and

$$\text{var} [y_{\mathbf{p}, \Xi}(\mathbf{X})] = \sum_{i=2}^{L_{\mathbf{p}, \Xi}} C_i^2 \leq \text{var} [y(\mathbf{X})], \quad \text{var} [y_{S, \mathbf{p}, \Xi}(\mathbf{X})] = \sum_{i=2}^{L_{S, \mathbf{p}, \Xi}} \bar{C}_i^2 \leq \text{var} [y(\mathbf{X})], \tag{63}$$

respectively.

6.2. Least-squares regression

The standard least-squares (SLS) regression is predicated on the best approximation properties of SCE and SDD methods, which are described, in the mean-square sense, by [32]

$$\mathbb{E} [y(\mathbf{X}) - y_{\mathbf{p}, \Xi}(\mathbf{X})]^2 = \inf_{g \in S_{\mathbf{p}, \Xi}} \mathbb{E} [y(\mathbf{X}) - g(\mathbf{X})]^2 \tag{64}$$

and

$$\mathbb{E} [y(\mathbf{X}) - y_{S, \mathbf{p}, \Xi}(\mathbf{X})]^2 = \inf_{h \in S_{S, \mathbf{p}, \Xi}} \mathbb{E} [y(\mathbf{X}) - h(\mathbf{X})]^2, \tag{65}$$

where $S_{p,\varepsilon}$ and $S_{S,p,\varepsilon}$ are relevant spline spaces. Therefore, the approximate expansion coefficients of $y_{p,\varepsilon}(\mathbf{X})$ and $y_{S,p,\varepsilon}(\mathbf{X})$ are determined from the minimizations of

$$\mathbb{E} \left[y(\mathbf{X}) - \sum_{i=1}^{L_p} C_i \phi_i(\mathbf{X}) \right]^2 \quad \text{and} \quad \mathbb{E} \left[y(\mathbf{X}) - \sum_{i=1}^{L_{S,p,\varepsilon}} \bar{C}_i \bar{\varphi}_i(\mathbf{X}) \right]^2. \quad (66)$$

Given a UQ problem with known distribution of random input \mathbf{X} and an output function $y : \mathbb{A}^N \rightarrow \mathbb{R}$, consider an input–output data set $\{\mathbf{x}^{(l)}, y(\mathbf{x}^{(l)})\}_{l=1}^L$ of size $L \in \mathbb{N}$. The mapping y can be as simple as an explicitly defined mathematical function or as intricate as an implicitly described function obtained via computational simulation, such as FEA of complex dynamical systems. In either case, the data set, often referred to as the experimental design, can be generated by calculating the function $y(\mathbf{x}^{(l)})$ at each input data point $\mathbf{x}^{(l)}$. Various sampling methods, namely, standard MCS, quasi MCS, and Latin hypercube sampling, can be used to build the experimental design.

According to SLS, the expansion coefficients of the SCE and SDD approximation are estimated by minimizing

$$\hat{e}_{p,\varepsilon} := \frac{1}{L} \sum_{l=1}^L \left[y(\mathbf{x}^{(l)}) - \sum_{i=1}^{L_{p,\varepsilon}} C_i \phi_i(\mathbf{x}^{(l)}) \right]^2 \quad (67)$$

and

$$\hat{e}_{S,p,\varepsilon} := \frac{1}{L} \sum_{l=1}^L \left[y(\mathbf{x}^{(l)}) - \sum_{i=1}^{L_{S,p,\varepsilon}} \bar{C}_i \bar{\varphi}_i(\mathbf{x}^{(l)}) \right]^2, \quad (68)$$

respectively, which are empirical analogs of Eq. (66). Denote by

$$\mathbf{A} := \begin{bmatrix} \phi_1(\mathbf{x}^{(1)}) & \cdots & \phi_{L_{p,\varepsilon}}(\mathbf{x}^{(1)}) \\ \vdots & \ddots & \vdots \\ \phi_1(\mathbf{x}^{(L)}) & \cdots & \phi_{L_{p,\varepsilon}}(\mathbf{x}^{(L)}) \end{bmatrix}, \quad \bar{\mathbf{A}} := \begin{bmatrix} \varphi_1(\mathbf{x}^{(1)}) & \cdots & \varphi_{L_{S,p,\varepsilon}}(\mathbf{x}^{(1)}) \\ \vdots & \ddots & \vdots \\ \varphi_1(\mathbf{x}^{(L)}) & \cdots & \varphi_{L_{S,p,\varepsilon}}(\mathbf{x}^{(L)}) \end{bmatrix}, \quad (69)$$

and

$$\mathbf{b} := (y(\mathbf{x}^{(1)}), \dots, y(\mathbf{x}^{(L)}))^T \quad (70)$$

an $L \times L_{p,\varepsilon}$ matrix, $L \times L_{S,p,\varepsilon}$ matrix, and L -dimensional column vector, respectively, comprising evaluations of the orthonormal spline basis functions from SCE and SDD approximations and output function at the data points, respectively. Then, the estimated coefficients \hat{C}_i , $i = 1, \dots, L_{p,\varepsilon}$, of SCE and $\hat{\bar{C}}_i$, $i = 1, \dots, L_{S,p,\varepsilon}$, of SDD are obtained as

$$\hat{\mathbf{c}} := (\hat{C}_1, \dots, \hat{C}_{L_{p,\varepsilon}})^T = (\mathbf{A}^T \mathbf{A})^{-1} \mathbf{A}^T \mathbf{b} \quad (71)$$

and

$$\hat{\bar{\mathbf{c}}} := (\hat{\bar{C}}_1, \dots, \hat{\bar{C}}_{L_{S,p,\varepsilon}})^T = (\bar{\mathbf{A}}^T \bar{\mathbf{A}})^{-1} \bar{\mathbf{A}}^T \mathbf{b}, \quad (72)$$

respectively. Here, $\mathbf{A}^T \mathbf{A}$ is an $L_{p,\varepsilon} \times L_{p,\varepsilon}$ matrix, while $\bar{\mathbf{A}}^T \bar{\mathbf{A}}$ is an $L_{S,p,\varepsilon} \times L_{S,p,\varepsilon}$ matrix; each of them is often referred to as the information or data matrix. A necessary condition for the SLS solution is $L > L_{p,\varepsilon}$ or $L > L_{S,p,\varepsilon}$, that is, the data size must be larger than the respective number of coefficients involved. Therefore, the computational cost of SCE/SDD approximations, which primarily comes from generating L samples of an output response, is directly proportional to the number of basis functions or coefficients, as alluded to in Section 5.3. Even when this condition is satisfied, the experimental design must be judiciously selected in such a way that the information matrices are well-conditioned.

In lieu of Eq. (66), different error measures are possible to estimate the SCE and SDD coefficients [39]. However, convergence properties associated with such error measures in the context of SCE/SDD approximations have yet to be studied rigorously.

7. Numerical examples

Two numerical examples illustrating the SCE and SDD approximations are presented for solving UQ problems in structural dynamics. The first example discusses frequency response analysis by SCE, whereas the second example addresses modal analysis by SDD. For the SCE/SDD methods, the degrees p_k and knot vectors ξ_k are identical in all coordinate directions. Therefore, the index k will be dropped when discussing the degrees p , knot vectors ξ , and number of subintervals I in this section. In addition, all knot vectors are $(p_k + 1)$ -open with simple (Examples 1 and 2) or repeated (Example 1) knots. Depending on the example, the knots are uniformly spaced and/or non-uniformly spaced. The optimal determination of these B-spline parameters, as demonstrated, for instance, using NURBS in a deterministic setting [39] and using SDD in a stochastic setting [40], was not pursued in this work.

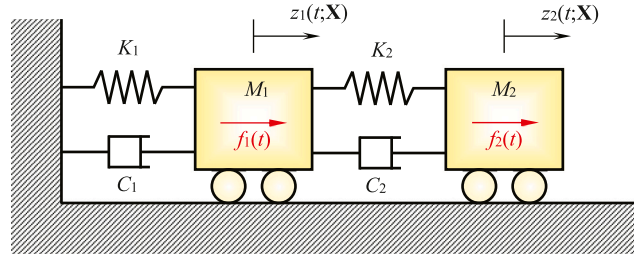


Fig. 1. A two-degree-of-freedom spring–mass–damper system.

7.1. Example 1: frequency response analysis of a two-degree-of-freedom system ($N = 1$ or 3)

Consider a two-degree-of-freedom, proportionally damped, dynamic system, shown in Fig. 1, with possibly random masses, damping coefficients, and spring constants

$$M_1 = M_2 = (1 + \delta_M X_M) \text{ kg}, \quad C_1 = C_2 = (1 + \delta_C X_C) \text{ N/(ms)},$$

$$\text{and } K_1 = K_2 = 15000(1 + \delta_K X_K) \text{ N/m},$$

respectively, where X_M , X_C , and X_K are independent, standard Gaussian random variables with δ_M , δ_C , and δ_K representing their corresponding coefficients of variation (COVs). By selecting appropriate values of the COVs, various dynamic systems, whether fully deterministic (all COVs = 0), fully random (all COVs $\neq 0$), or a random-deterministic combination (some COVs = 0), can be studied. Therefore, for a fully random dynamic system, the input random vector $\mathbf{X} = \{X_M, X_C, X_K\}^T$.

The dynamic system is subjected to a harmonic excitation force vector $\mathbf{f}(t) = \mathbf{F}_\omega \exp(i\omega t)$ with the force amplitude vector $\mathbf{F} = \{1, 0\}^T$ N and angular frequency $20\pi \leq \omega \leq 70\pi$ rad/s. In terms of ordinary frequency $f := \omega/(2\pi)$, the range is $10 \leq f \leq 35$ Hz. From linear dynamics, the steady-state displacement response vector is $\mathbf{z}(t) = \mathbf{Z}(\omega; \mathbf{X}) \exp(i\omega t)$, where the complex-valued displacement amplitude vector $\mathbf{Z}(\omega; \mathbf{X}) = (Z_1(\omega; \mathbf{X}), Z_2(\omega; \mathbf{X}))^T$ satisfies

$$\left(-\omega^2 \begin{bmatrix} M_1 & 0 \\ 0 & M_2 \end{bmatrix} + i\omega \begin{bmatrix} C_1 + C_2 & -C_2 \\ -C_2 & C_2 \end{bmatrix} + \begin{bmatrix} K_1 + K_2 & -K_2 \\ -K_2 & K_2 \end{bmatrix} \right) \begin{pmatrix} Z_1(\omega; \mathbf{X}) \\ Z_2(\omega; \mathbf{X}) \end{pmatrix} = \begin{pmatrix} 1 \\ 0 \end{pmatrix}. \tag{73}$$

The objective of this example is to calculate the second-moment statistics and probability distributions of $|Z_1(\omega; \mathbf{X})|$ or $|Z_1(2\pi f; \mathbf{X})|$ by PCE and SCE for a range of frequencies due to the uncertainty in system properties.

For UQ analysis, the basis functions of PCE are orthonormal Hermite polynomials that are consistent with the standard Gaussian probability distribution of input random variables. In contrast, the basis functions of SCE are orthonormal splines that are consistent with the truncated Gaussian probability distribution on the bounded domain $[-3, +3]^N$ of input random variables. In addition, for SCE, the output function was transformed to a function of truncated Gaussian variable by matching the CDFs of standard and truncated Gaussian variables. It is necessary to do so because splines require bounded support by definition. It is best practice to select a transformation yielding as little difference between the original and mapped distributions as is possible. Hence, the truncated Gaussian distribution is an appropriate choice for the transformation.

All expansion coefficients of PCE and SCE were calculated from their respective definitions, requiring N -dimensional integrations, such as Eq. (34) from SCE. These integrals were subsequently estimated by respective Gauss quadrature rules for both PCE and SCE, where the quadrature in the latter was performed in each subinterval determined by the chosen knot vector. Therefore, the following results of PCE and SCE are due to not only their respective projections, but also due to numerical approximations of expansion coefficients. No detailed numerical study was performed to eliminate the error from the latter.

Two distinct cases, one considering the randomness of the spring stiffness only ($N = 1$) and the other allowing the randomness of mass, damping, and stiffness properties ($N = 3$), were studied. For the mean input in both cases, the natural (ordinary) frequencies are $f_1 := \omega_1/(2\pi) = 12.047$ Hz and $f_2 := \omega_2/(2\pi) = 31.539$ Hz.

7.1.1. Case 1: randomness in stiffness only ($N = 1$)

For the first case, set $\delta_M = \delta_C = 0$ and $\delta_K = 0.05$, and assume X_K to be a standard Gaussian random variable with zero mean and standard deviation of one. Therefore, the system has deterministic masses $M_1 = M_2 = 1$ kg, deterministic damping coefficients $C_1 = C_2 = 1$ N/(ms), and random spring constants $K_1 = K_2 = 15000(1 + 0.05X_K)$ N/m. There is only one input random variable, so that $\mathbf{X} = \{X_K\}$ and $N = 1$. Although the Gaussian assumption theoretically allows a negative value of spring stiffness, the probability of such event is very low, given the smallness (5%) of the COV used. Moreover, such an assumption permits a fair comparison with past studies [20,21], where the old results can be compared with the new ones produced from this work.

Five UQ methods — a 50th-order PCE ($m = 50$), two linear or first-order SCEs ($p = 1, I = 8; p = 1, I = 16$), two quadratic or second-order SCEs ($p = 2, I = 8; p = 2, I = 16$) — along with crude MCS (100,000 samples) as a benchmark solution were employed to calculate the statistical properties of $|Z_1(2\pi f; X_K)|$ for this one-dimensional UQ problem. Here, p and I refer to the B-spline order and the number of subintervals, respectively, of SCE. Table 2 lists both instances of uniformly spaced and non-uniformly

Table 2
Uniformly spaced and non-uniformly spaced knot vectors for the SCE approximations in Example 1.

SCE method	Knot vector
(a) Uniformly spaced knots	
1st-order ($p = 1, I = 8$)	$\xi = \{-3, -3, -2.25, -1.5, -0.75, 0, 0.75, 1.5, 2.25, 3, 3\}$
1st-order ($p = 1, I = 16$)	$\xi = \{-3, -3, -2.625, -2.25, -1.875, -1.5, -1.125, -0.75, -0.375, 0, 0.375, 0.75, 1.125, 1.5, 1.875, 2.25, 2.625, 3, 3\}$
2nd-order ($p = 2, I = 8$)	$\xi = \{-3, -3, -3, -2.25, -1.5, -0.75, 0, 0.75, 1.5, 2.25, 3, 3, 3\}$
2nd-order ($p = 2, I = 16$)	$\xi = \{-3, -3, -3, -2.625, -2.25, -1.875, -1.5, -1.125, -0.75, -0.375, 0, 0.375, 0.75, 1.125, 1.5, 1.875, 2.25, 2.625, 3, 3, 3\}$
(b) Non-uniformly spaced knots	
1st-order ($p = 1, I = 8$)	$\xi = \{-3, -3, -1.5, -0.65, -0.25, 0, 0.25, 0.65, 1.5, 3, 3\}$
1st-order ($p = 1, I = 16$)	$\xi = \{-3, -3, -2.25, -1.75, -1.25, -0.8, -0.4, -0.25, -0.1, 0, 0.1, 0.25, 0.4, 0.8, 1.25, 1.75, 2.25, 3, 3\}$
2nd-order ($p = 2, I = 8$)	$\xi = \{-3, -3, -3, -1.5, -0.65, -0.25, 0, 0, 0.25, 0.65, 1.5, 3, 3, 3\}$
2nd-order ($p = 2, I = 16$)	$\xi = \{-3, -3, -3, -2.25, -1.75, -1.25, -0.8, -0.4, -0.25, -0.1, 0, 0, 0.1, 0.25, 0.4, 0.8, 1.25, 1.75, 2.25, 3, 3, 3\}$

spaced knots considered in this example. For linear SCEs ($p = 1$), all knot vectors comprise simple knots, whereas for quadratic SCEs ($p = 2$), the knot vectors have either uniformly spaced simple knots or non-uniformly spaced repeated knots. The need for a very high-order PCE is justified based on past works [20,21], where lower-order expansions provided vastly erroneous results. The number of polynomial basis functions required by the PCE approximation is 51, whereas only 9 or 17 spline basis functions are involved in the first-order ($p = 1$) SCE approximations associated with $I = 8$ and $I = 16$, respectively. For the second-order ($p = 2$) SCE methods, there are 10 or 18 basis functions for uniformly spaced knots and 11 or 19 basis functions for non-uniformly spaced knots for $I = 8$ and $I = 16$, respectively. The expansion coefficients were estimated by numerical integration as follows: for PCE coefficients, the $(m + 20)$ -point Gauss-Hermite quadrature rule was employed, whereas for SCE coefficients, the Gauss-Legendre quadrature rule was used with $p + 20$ Gauss points on each subinterval of the knot vectors defined.

Figs. 2(a) and 2(b) present the plots of the standard deviations of $|Z_1(2\pi f; X_K)|$ for the range of external (ordinary) frequency f between 10 and 35 Hz, obtained by the abovementioned SCE approximations with uniformly spaced knots and non-uniformly spaced knots, respectively. The PCE estimates, also shown in both figures, are in good agreement with the MCS results only for the non-resonant frequencies. In the vicinity of the resonant frequencies (12.047 Hz, 31.539 Hz), PCE, even with such a high order, exhibits spurious oscillations that have no physical meaning. Displayed on the right by the enlarged views of the parts of these plots, such oscillations are more pronounced in the neighborhood of the lower natural frequency. This is primarily because FRFs are non-smooth functions, emanating from sudden changes of the amplitude that occur around resonant frequencies. For instance, when $|Z_1(2\pi f_1; x_K)|$, determined at $f = f_1 = 12.047$ Hz, is plotted against the real variable x_K , the non-smoothness at $x_K = 0$ is clearly visible in Figs. 3(a) or 3(b). In contrast, the PCE approximation of $|Z_1(2\pi f_1; x_K)|$, also presented in the aforementioned figures, is smooth and oscillatory, despite the use of an ultra high-order ($m = 50$) expansion. Note that the harshness of the actual response function in the vicinity of the resonant frequencies also makes the numerical integration, required to estimate the high-order PCE coefficients, daunting. To reduce the magnitudes of such oscillations, an impractically large-order PCE as well as an extremely accurate numerical integration scheme are required, which are computationally prohibitive for large-scale systems. On the other hand, the SCE-generated function approximations and standard deviations, also plotted in the two foregoing sets of figures, demonstrate more stable behavior by markedly reducing the oscillations around the resonant frequencies. For quadratic ($p = 2$) SCE methods, the approximations [Fig. 3(b)] improve significantly by using repeated knots at $x_K = 0$, which is due to the nonsmoothness of the original function at $x_K = 0$. For non-uniformly spaced knots, the SCE and MCS results are nearly coincident or extremely close to each other, regardless of the approximation order or the number of subintervals. This is possible because splines are more flexible than polynomials in selecting expansion orders and dealing with subdomains. In consequence, low-degree SCE approximations with appropriate knot vectors produce results superior to those of high-order PCE approximations. Furthermore, SCE achieves this feat using at most nearly a third of the number of basis functions mandated by PCE.

Once the aforementioned PCE and SCE approximations are constructed, they are re-sampled 100,000 times, facilitating calculation of the PDF or CDF of $|Z_1(2\pi f_1; X_K)|$ at the chosen frequency of $f = f_1 = 12.047$ Hz. Figs. 4(a) and 4(b) exhibit the plots of such PDFs and CDFs, where the SCE results are reported separately for uniformly spaced knots and non-uniformly spaced knots, respectively. The comparisons with the CDF/PDF generated by crude MCS (100,000 samples), also depicted in these figures, indicate that SCE calculates the probabilistic characteristics of FRFs, especially at the tail region, more accurately than PCE as well, provided that the number of subintervals is adequately large ($I = 16$) for either linear or quadratic SCE. Furthermore, the quality of SCE results enhances substantially when non-uniformly spaced knots [Fig. 4(b)] are used as opposed to uniformly spaced knots [Fig. 4(a)]. This is obviously due to SCE's finer approximation quality with non-uniformly spaced knots and the presence of repeated knots for quadratic SCE approximations of non-smooth functions, as established in Fig. 3(b). Indeed, given the harshness of the functions under study, the SCE results are convergent with the increase in the number of subintervals, and quadratic SCE ($p = 2, I = 16$) outperforms the 50th-order PCE. Hence, the proposed SCE method is extremely powerful in handling random functions, especially those involving non-smoothness or heavily oscillatory behavior.

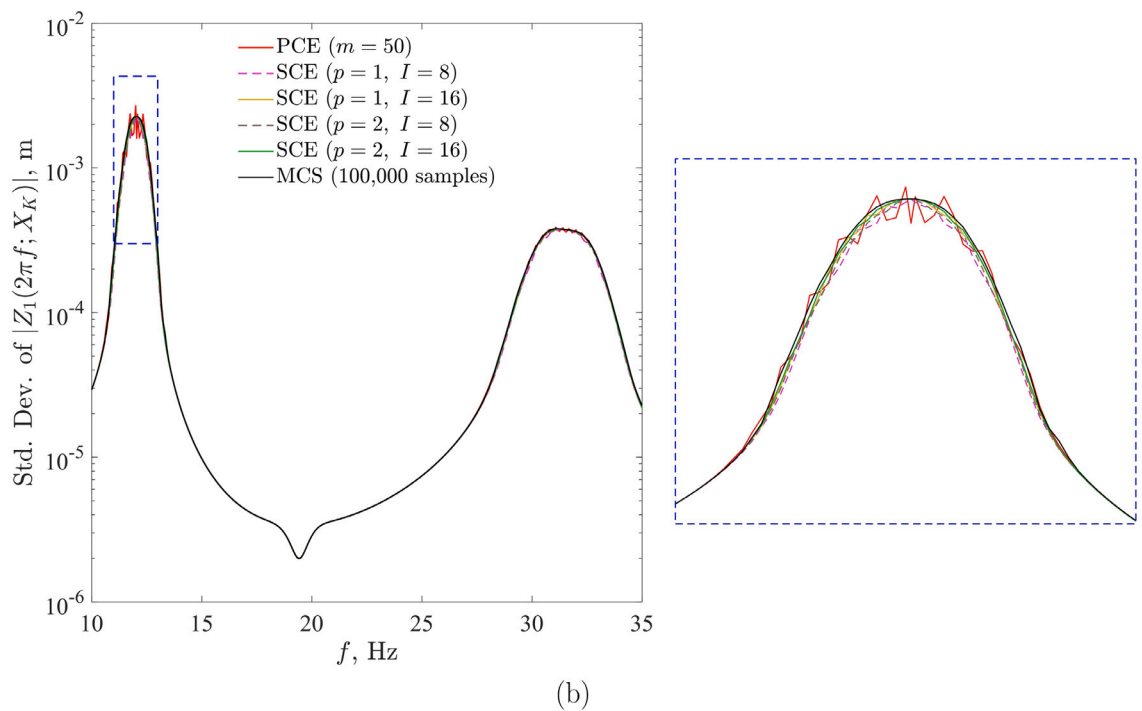
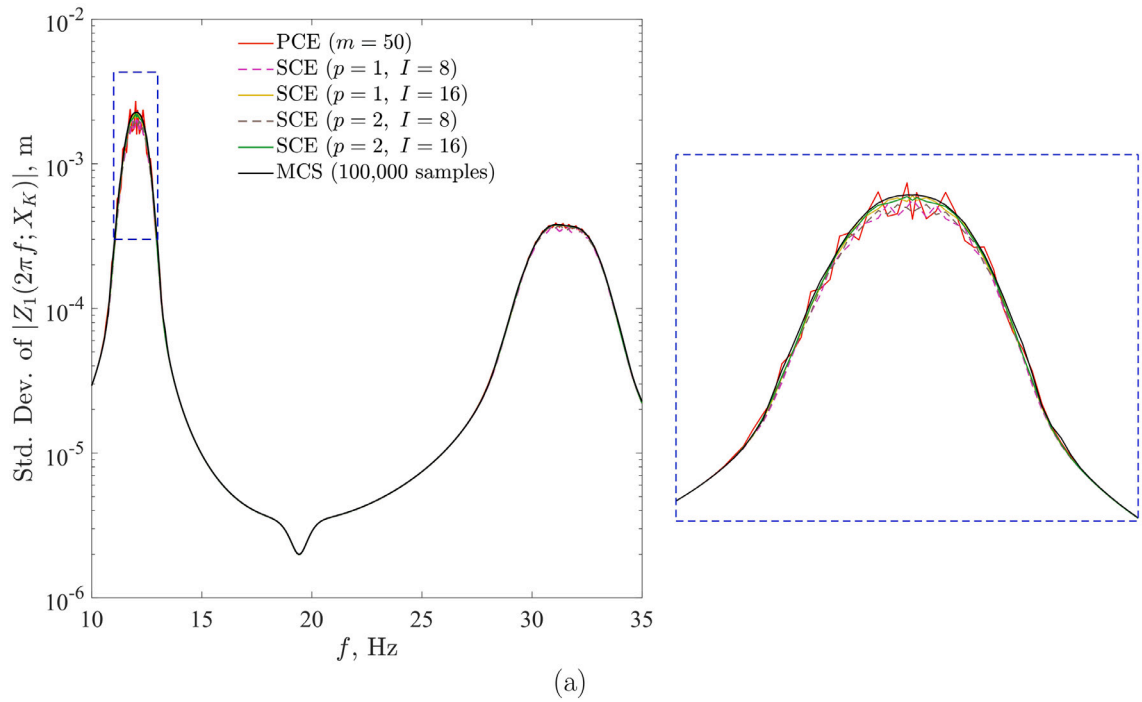


Fig. 2. Standard deviations of $|Z_1(2\pi f; X_K)|$ for $10 \leq f \leq 35$ Hz obtained by SCE and other methods for Case 1: (a) uniformly spaced knots; (b) non-uniformly spaced knots.

7.1.2. Case 2: randomness in mass, damping, and stiffness ($N = 3$)

The second case involves modeling mass, damping, and stiffness to be all random variables, that is, $M_1 = M_2 = (1 + 0.05X_M)$ kg, $C_1 = C_2 = (1 + 0.05X_C)$ N/(ms), and $K_1 = K_2 = 15000(1 + 0.05X_K)$ N/m, obtained by selecting $\delta_M = \delta_C = \delta_K = 0.05$. Therefore, there

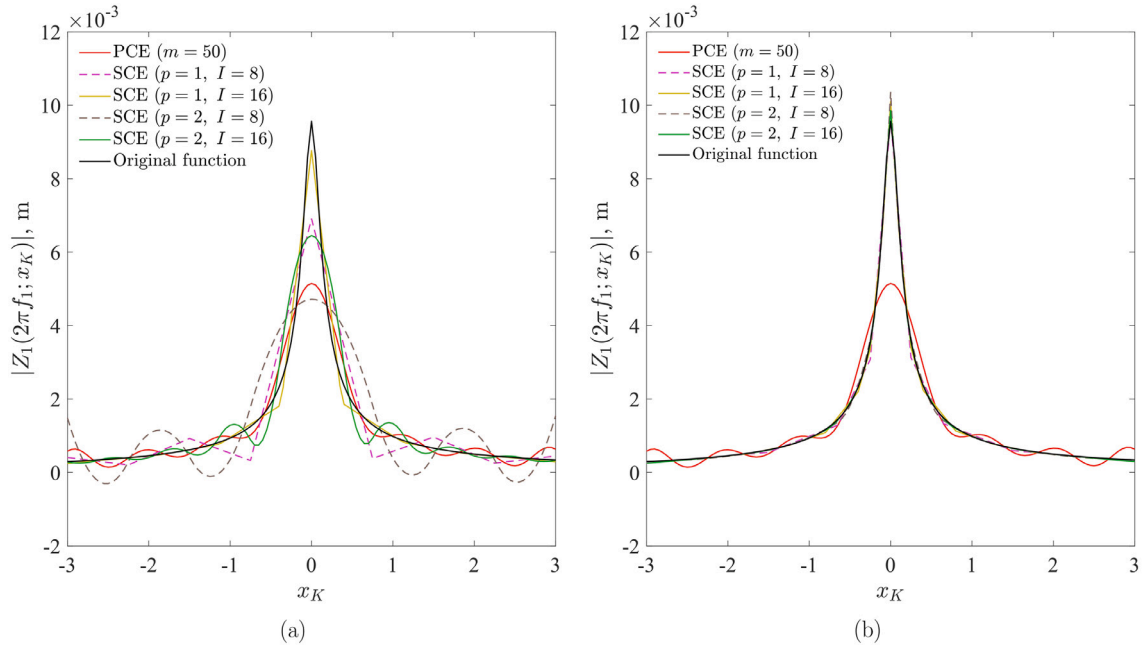


Fig. 3. $|Z_1(2\pi f_1; x_K)|$ at $f = f_1 = 12.047$ Hz vs. x_K and its approximations by SCE and PCE for Case 1: (a) uniformly spaced knots; (b) non-uniformly spaced knots.

are three input random variables, so that $\mathbf{X} = \{X_M, X_C, X_M\}^T$ and $N = 3$. All three random variables are mutually independent and follow standard Gaussian probability distributions.

Fig. 5(a) and 5(b) feature similar plots of the second-moment properties of $|Z_1(2\pi f; \mathbf{X})|$ for the aforementioned range of frequencies, obtained using (1) a 20th-order PCE ($m = 20$), (2) a first-order SCE ($p = 1, I = 8$), and (3) a relatively finer first-order SCE ($p = 1, I = 16$). Once again, uniformly spaced and non-uniformly spaced simple knots as those defined in Table 1 are used in the SCE approximations, where the B-spline order (p) and the number of subintervals (I) are identical in all coordinate directions $k = 1, 2, 3$ of the stochastic domain. The numbers of respective basis functions by the PCE ($m = 20$), SCE ($p = 1, I = 8$), and SCE ($p = 1, I = 16$) methods are 9261, 729, and 4913, respectively. All expansion coefficients were calculated using tensor-products of ($m + 5$)- or ($p + 5$)-point Gauss-Hermite or Gauss-Legendre quadrature rules for PCE or SCE coefficients, respectively, where $p + 5$ is associated with each subinterval of the knot vectors used in SCE. When compared with the results of crude MCS (100,000 samples), SCE for this three-dimensional UQ problem also substantially reduces oscillations around the resonant frequencies, whereas PCE continues to struggle. Once again, SCE outperforms PCE, using significantly fewer basis functions than those required by the latter. Indeed, the results of both Cases 1 and 2, which are qualitatively the same, reveal greater approximation quality of splines over polynomials.

Despite the success of SCE in probabilistic analysis of FRFs, its application is limited to solving low-dimensional UQ problems ($N < 10$). For high-dimensional problems ($N > 10$), SCE becomes computationally prohibitive, raising the need for SDD as a practical remedy. The SDD will be featured next in the context of modal analysis.

7.2. Example 2: modal analysis of Dassault Rafale fighter jet ($N = 110$)

The second example delves into solving a practical UQ problem in tandem with modal analysis of a Dassault Rafale fighter jet introduced in 2001 [42]. The problem is large-scale, as there are 110 random variables, and the aim is to quantify the uncertainties in the natural frequencies and mode shapes of the jet by means of the proposed SDD method. The principal objective is to investigate the accuracy and efficiency of the SDD method in solving this industrial-scale engineering problem.

A picture of the actual jet is shown in Fig. 6(a). While the material composition of the jet is not publicly available in detail, Fig. 6(b) uses color coding to illustrate 11 types of materials considered for use in manufacturing the different parts of the jet. The materials, including Kevlar, composite, Aluminum 2024 alloy, and Titanium Ti6Al4V alloy, are all common in the aerospace industry. All 11 materials have orthotropic elastic properties. According to the data provided in Table 3, each material has three random Young's moduli E_x , E_y , and E_z in GPa, three random shear moduli G_{xy} , G_{xz} , and G_{yz} in GPa, three random Poisson's ratios ν_{xy} , ν_{xz} , and ν_{yz} , and one random mass density ρ in kg/m^3 , adding up to 10 random variables. No damping is included. Therefore, there are 110 random variables in this UQ problem. Such high-dimensional problems are extremely challenging and provide an onerous test for the SDD method.

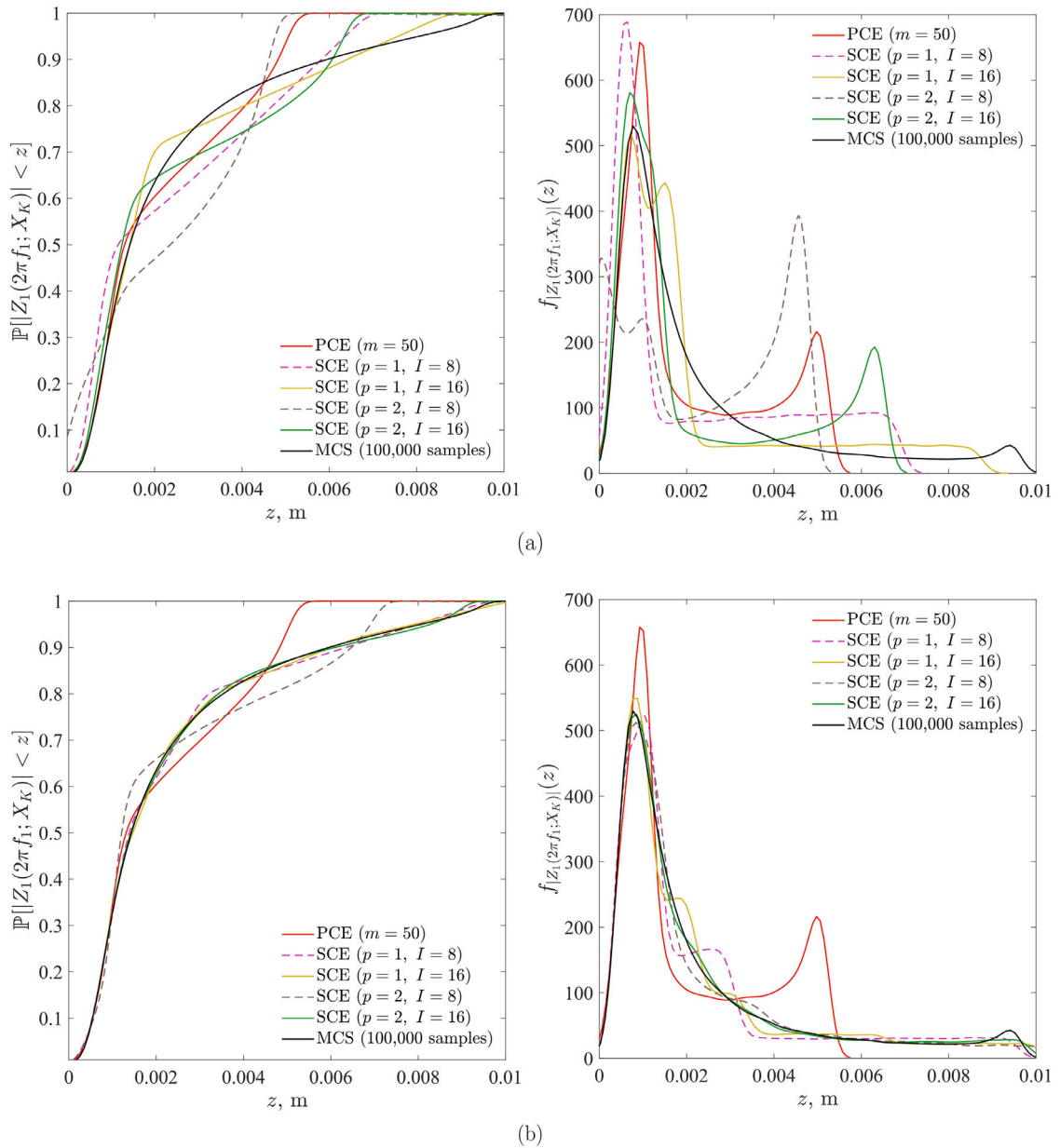


Fig. 4. CDF and PDF of $|Z_1(2\pi f_1; X_K)|$ at $f = f_1 = 12.047$ Hz obtained by SCE and other methods for Case 1: (a) uniformly spaced knots; (b) non-uniformly spaced knots.

In reference to Assumption 1, recall that for an SDD method to be applicable, all probability distributions of input random variables must be defined on bounded domains $[a_k, b_k]$, $k = 1, \dots, 110$.³ The mass densities in Table 3 all follow truncated Gaussian distributions, while the Young’s moduli, the shear moduli, and the Poisson’s ratios all have uniform probability distributions. For each material in Table 3, the mean, COV, and bound limits $[a, b]$ are defined for $E_x, E_y, E_z, G_{xy}, G_{xz}, G_{yz}, \nu_{xy}, \nu_{xz}, \nu_{yz}$, and ρ . In the table, the subscript k has been dropped from a_k and b_k for brevity.

As the deterministic black-box solver, an FEA model, with the mesh delineated in Fig. 6(c), was developed using ABAQUS (Version 2019) [43]. The model consists of 30,869 linear tetrahedral elements and 9247 nodes and was not constrained to mimic free-free vibration. Note that the problem was solved for a fixed FEA model. In other words, the impact of ABAQUS mesh refinement on

³ If an input random variable has unbounded distribution, then a transformation to a random variable with bounded distribution is required. For further details, the readers are referred to a prior work by the authors [38].

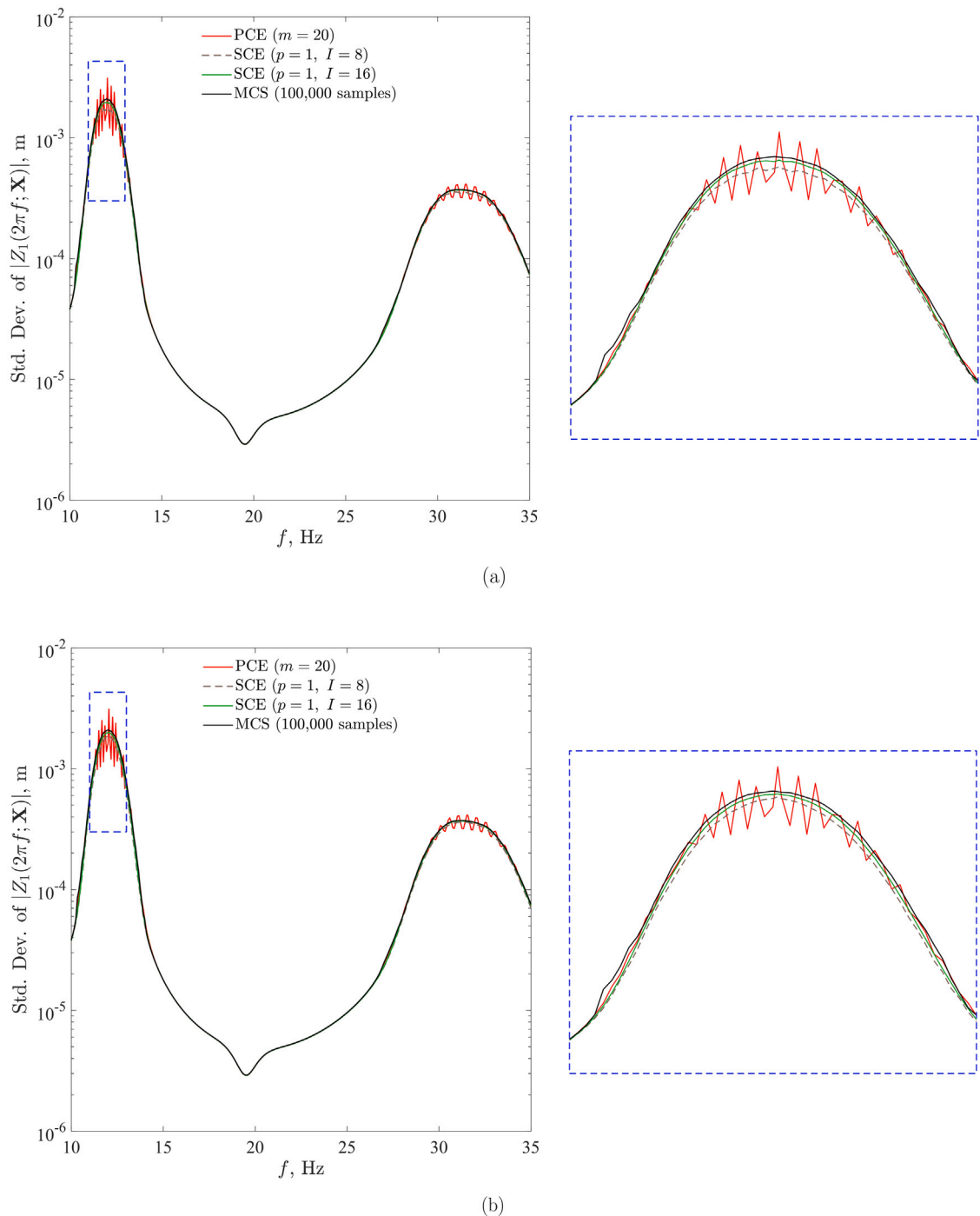


Fig. 5. Standard deviations of $|Z_1(2\pi f; \mathbf{X})|$ for $10 \leq f \leq 35$ Hz obtained by SCE and other methods for Case 2: (a) uniformly spaced knots; (b) non-uniformly spaced knots.

the quality of the results was not studied. Nevertheless, the model demonstrated in Fig. 6(c) was deemed satisfactory in terms of accuracy and computational expediency. To solve for the natural frequencies and mode shapes, the standard Lanczos method [44] was employed.

For UQ analysis, the statistical moments of the natural frequencies and mode shapes were estimated by crude MCS with 10,000 samples (FEA) as the benchmark solution and three univariate SDD methods, comprising two of linear orders ($p = 1, I = 2, 4$) and one of the quadratic order ($p = 2, I = 4$). Here, p and I refer to the B-spline order and the number of subintervals, equal in

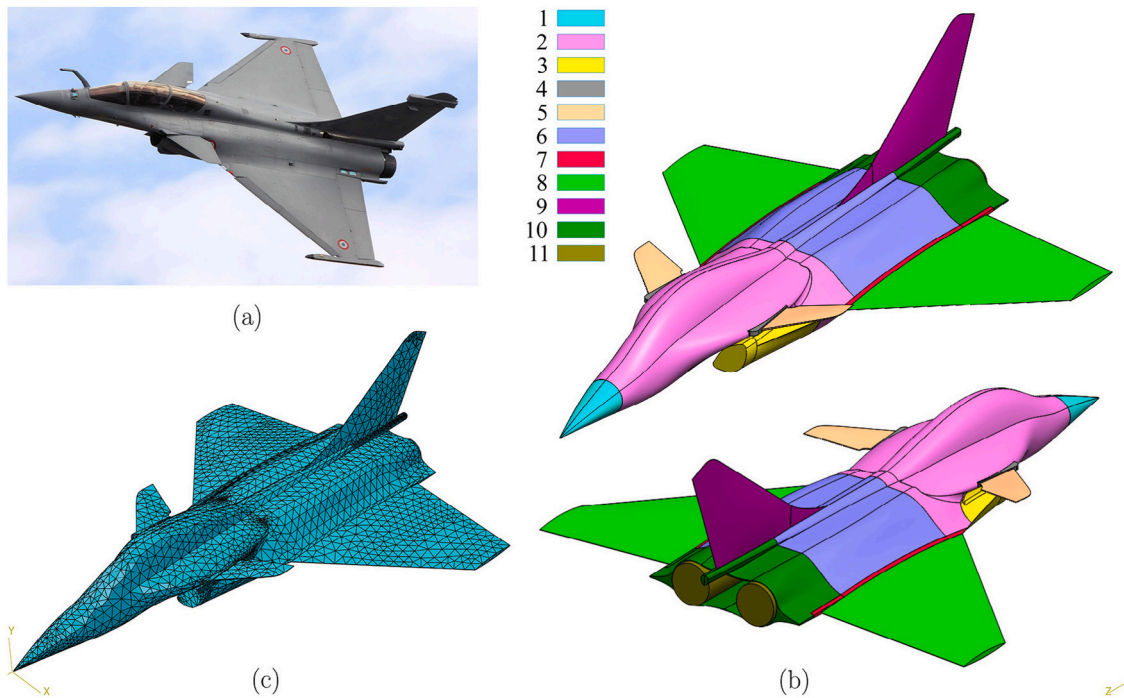


Fig. 6. Dassault Rafale fighter jet problem [42]: (a) the actual jet; (b) a CAD model showing eleven materials; and (c) an FEA model. (For interpretation of the references to color in this figure legend, the reader is referred to the web version of this article.)

all coordinate directions $k = 1, \dots, 110$ of the stochastic domain. Moreover, only univariate SDD methods would be affordable to efficiently solve this ultra high-dimensional UQ problem. In other words, $S = 1$ in all three SDD methods described earlier. Overall, there were 221, 441, and 551 basis functions in the SDD ($p = 1, I = 2$), SDD ($p = 1, I = 4$), and SDD ($p = 2, I = 4$) methods, respectively.

The SDD coefficients were estimated by the SLS regression with the data size being slightly more than *four* times the number of basis functions used by the SDD methods. Note that although there are some rules of thumb for how many samples to pick for regression purposes, there is no perfect suggestion that would guarantee obtaining good results by SLS. Eventually, 972, 1940, and 2424 samples (FEA) were used for estimating the expansion coefficients of the SDD ($p = 1, I = 2$), SDD ($p = 1, I = 4$), and SDD ($p = 2, I = 4$) methods, respectively, which are larger than four times the number of basis functions for each SDD method.

The results will be presented in two subsections: one for the second-moment analysis of the natural frequencies and mode shapes, and the other for the CDF analysis of an output random variable of interest.

7.2.1. Second-moment analysis

As the FEA model was not constrained, the first six mode shapes correspond to rigid-body motions with their associated frequencies practically *zero*. Therefore, Table 4 lists the means and standard deviations of the first ten non-rigid-body natural frequencies of the jet computed by the crude MCS and three SDD methods. As observed from the table, there is an outstanding match between the results obtained by all three SDD methods and those provided by crude MCS as the reference solution. Moreover, the mean values are estimated more accurately, which is expected, since in UQ, relatively higher-order moments – standard deviation in this case – are generally more challenging to accurately compute. Nevertheless, the SDD methods are able to economically estimate the second-moment statistical properties of the natural frequencies. For instance, the SDD ($p = 1, I = 2$) method does so by using only 972 samples (FEA), which is less than one tenth of the number of FEA employed by MCS.

Figs. 7 and 8 illustrate the standard deviations of the fifth and sixth non-rigid-body mode shapes, respectively, calculated by MCS and three SDD methods. Consistent with the results of natural frequencies in Table 4, the contour plots are generally similar, although those of the SDD ($p = 2, I = 4$) method are the closest to their MCS counterparts. This match between the SDD ($p = 2, I = 4$) and MCS methods is more perceptible to the naked eye in Fig. 8. Hence, the proposed SDD method is able to accurately and efficiently estimate the second statistical moments of the outputs of interest for this 110-dimensional problem by taking advantage of the dimensionwise expansion of the random function.

Table 3
Mean, COV, and bound limits associated with the random material properties for the jet problem.

Material	Type		E_x (GPa)	E_y (GPa)	E_z (GPa)	G_{xy} (GPa)	G_{xz} (GPa)	G_{yz} (GPa)	ν_{xy}	ν_{xz}	ν_{yz}	ρ (kg/m ³)	
1	Kevlar	Mean	65.2	78.4	51.9	24.1	36.4	27.4	0.41	0.38	0.32	1440	
		COV	0.06	0.06	0.06	0.06	0.06	0.06	0.06	0.06	0.06	0.06	0.05
		<i>a</i>	58.7	70.6	46.7	21.7	32.8	24.7	0.37	0.34	0.29	1152	
		<i>b</i>	71.7	86.2	57.1	26.5	40.0	30.1	0.45	0.42	0.35	1728	
2	Composite	Mean	441	409	462	167	190	171	0.32	0.38	0.33	1870	
		COV	0.06	0.06	0.06	0.06	0.06	0.06	0.06	0.06	0.06	0.06	0.08
		<i>a</i>	397	368	416	151	171	154	0.29	0.34	0.30	1403	
		<i>b</i>	485	450	508	184	209	188	0.35	0.42	0.36	2338	
3	Aluminum 2024	Mean	62.1	78.7	70.3	28.8	38.0	23.5	0.29	0.23	0.25	2781	
		COV	0.09	0.09	0.09	0.09	0.09	0.09	0.09	0.09	0.09	0.09	0.1
		<i>a</i>	52.8	66.9	59.8	24.5	32.3	20.0	0.25	0.20	0.21	1947	
		<i>b</i>	71.4	90.5	80.8	33.1	43.7	27.0	0.33	0.26	0.29	3615	
4	Aluminum 2024	Mean	71.8	84.0	63.9	29.1	23.5	32.3	0.27	0.31	0.26	2653	
		COV	0.06	0.06	0.06	0.06	0.06	0.06	0.06	0.06	0.06	0.06	0.1
		<i>a</i>	64.6	75.6	57.5	26.2	21.2	29.1	0.24	0.28	0.23	1857	
		<i>b</i>	79.0	92.4	70.3	32.0	25.9	35.5	0.30	0.34	0.29	3449	
5	Titanium Ti6Al4V	Mean	121.7	103.6	107.7	35.5	48.2	42	0.31	0.28	0.34	4407	
		COV	0.12	0.12	0.12	0.12	0.12	0.12	0.12	0.12	0.12	0.1	
		<i>a</i>	97.4	82.9	86.2	28.4	38.6	33.6	0.25	0.22	0.27	3085	
		<i>b</i>	146	124	129	42.6	57.8	50.4	0.37	0.34	0.41	5729	
6	Aluminum 2024	Mean	67.5	70.9	78.4	33.1	30.9	26.2	0.37	0.34	0.28	2835	
		COV	0.06	0.06	0.06	0.06	0.06	0.06	0.06	0.06	0.06	0.08	
		<i>a</i>	60.8	63.8	70.6	29.8	27.8	23.6	0.33	0.31	0.25	1985	
		<i>b</i>	74.2	78.0	86.2	36.4	34.0	28.8	0.41	0.37	0.31	3686	
7	Kevlar	Mean	79.9	66.8	70.0	27.6	25.3	21.9	0.41	0.38	0.32	1389	
		COV	0.09	0.09	0.09	0.09	0.09	0.09	0.09	0.09	0.09	0.05	
		<i>a</i>	67.9	56.8	59.5	23.5	21.5	18.6	0.35	0.32	0.27	1111	
		<i>b</i>	91.9	76.8	80.5	31.7	29.1	25.2	0.47	0.44	0.37	1667	
8	Composite	Mean	410	463	457	159	177	142	0.33	0.32	0.27	1935	
		COV	0.06	0.06	0.06	0.06	0.06	0.06	0.06	0.06	0.06	0.08	
		<i>a</i>	369	417	412	143	159	127	0.30	0.29	0.24	1451	
		<i>b</i>	451	510	503	175	194	156	0.36	0.35	0.30	2419	
9	Composite	Mean	423	451	434	166	177	155	0.29	0.35	0.32	1903	
		COV	0.06	0.06	0.06	0.06	0.06	0.06	0.06	0.06	0.06	0.08	
		<i>a</i>	380	406	391	149	159	140	0.26	0.32	0.29	1427	
		<i>b</i>	465	497	477	183	194	171	0.32	0.39	0.35	2379	
10	Kevlar	Mean	69.9	59.3	63.1	25.5	22.4	29.8	0.39	0.41	0.37	1463	
		COV	0.09	0.09	0.09	0.09	0.09	0.09	0.09	0.09	0.09	0.05	
		<i>a</i>	59.4	50.4	53.6	21.7	19.0	25.3	0.33	0.35	0.31	1170	
		<i>b</i>	80.4	68.2	72.6	29.3	25.8	34.3	0.45	0.47	0.43	1756	
11	Aluminum 2024	Mean	72.8	66.3	61.9	29.9	25.7	35.3	0.25	0.26	0.29	2859	
		COV	0.12	0.12	0.12	0.12	0.12	0.12	0.12	0.12	0.12	0.1	
		<i>a</i>	58.2	53.0	49.5	23.9	20.6	28.2	0.20	0.21	0.23	2001	
		<i>b</i>	87.4	79.6	74.3	35.9	30.8	42.4	0.30	0.31	0.35	3717	

7.2.2. CDF analysis

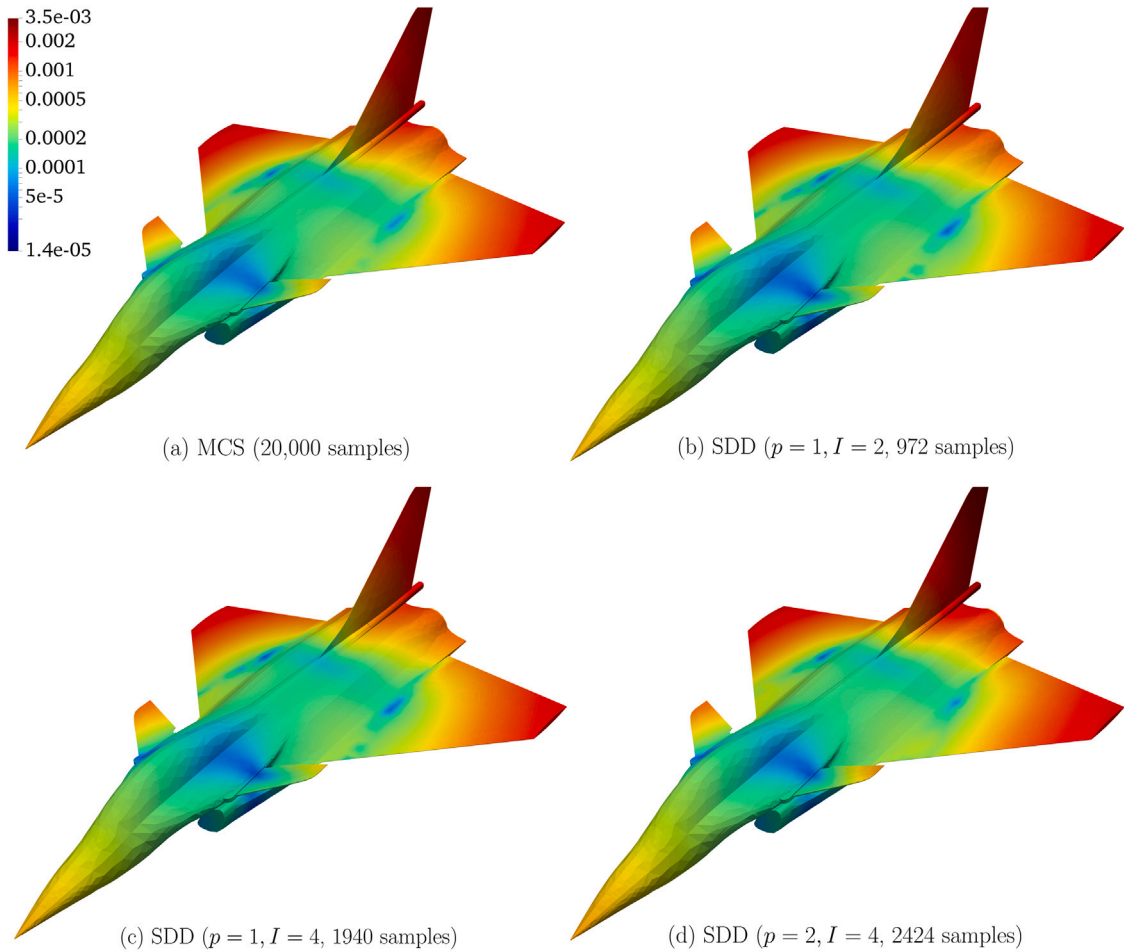
The results presented in the previous section cover only up to the second-order statistical moment, namely mean and standard deviation. However, in many applications, the PDF or CDF are required because they include all statistical moments of an output random variable of interest and important probabilistic information. The CDF is generally challenging to efficiently calculate by the UQ methods, especially in a tail region, which is crucial for evaluating probability of failure, including applications to design optimization.

Fig. 9 presents four estimates of the CDF of the first non-rigid-body mode natural frequency, denoted by $F_{f_1}(f_{1,0}) := \mathbb{P}[f_1 \leq f_{1,0}]$. The CDF curves generated by the MCS and SDD methods match very well and are consistent with the second-moment statistics provided in the previous section. In addition, SLS has proven to be successful in providing accurate estimates of the expansion coefficients. For the SDD methods, however, the CDFs do not change significantly by increasing either p or I . This clearly shows that the proposed SDD method can handle this UQ problem by using very low-order basis functions and only 2 or 4 subintervals. Evidently, this is because the original function under study is dominantly univariate. In other words, by truncating the SDD expansion at $S = 1$ and retaining only the univariate component functions, not much is lost in terms of accuracy. However, even solving such a problem using the PCE and SCE methods would have been impossible due to the curse of dimensionality, as these methods are

Table 4

Mean and standard deviation values of the first ten non-rigid-body frequencies of the jet by various methods.

Mode	Univariate SDD methods ^a						Crude MCS ^a	
	$p = 1, I = 2$		$p = 1, I = 4$		$p = 2, I = 4$		(10,000 samples)	
	Mean	St. dev.	Mean	St. dev.	Mean	St. dev.	Mean	St. dev.
1	44.614	2.343	44.614	2.349	44.614	2.351	44.609	2.412
2	45.033	2.331	45.039	2.338	45.039	2.338	45.032	2.395
3	49.344	2.332	49.345	2.334	49.344	2.334	49.342	2.391
4	50.463	2.608	50.466	2.613	50.465	2.614	50.462	2.669
5	71.979	2.417	71.980	2.401	71.978	2.402	71.963	2.477
6	80.128	1.589	80.103	1.603	80.098	1.668	80.088	1.677
7	82.177	1.779	82.207	1.776	82.213	1.839	82.177	1.829
8	90.364	2.982	90.379	2.994	90.377	3.025	90.335	2.998
9	101.25	5.154	101.25	5.187	101.26	5.207	101.24	5.206
10	109.54	5.739	109.55	5.756	109.55	5.756	109.53	5.769

^aAll frequencies are reported in Hz.**Fig. 7.** Standard deviation contour plot of the fifth non-rigid-body mode shape.

hindered, if not prohibited, when the stochastic dimension is generally greater than 10. The bottom line here is that the proposed SDD method can solve very high-dimensional UQ problems accurately and economically.

Notwithstanding the achievement of the univariate SDD approximations in this particular example, it is possible that higher-variate SDD approximations, prominently, the bivariate SDD approximations, may be required in other applications [30]. In this case, the computational effort of SDD will slowly ramp up, pointing to a need for further improvement in efficiency.

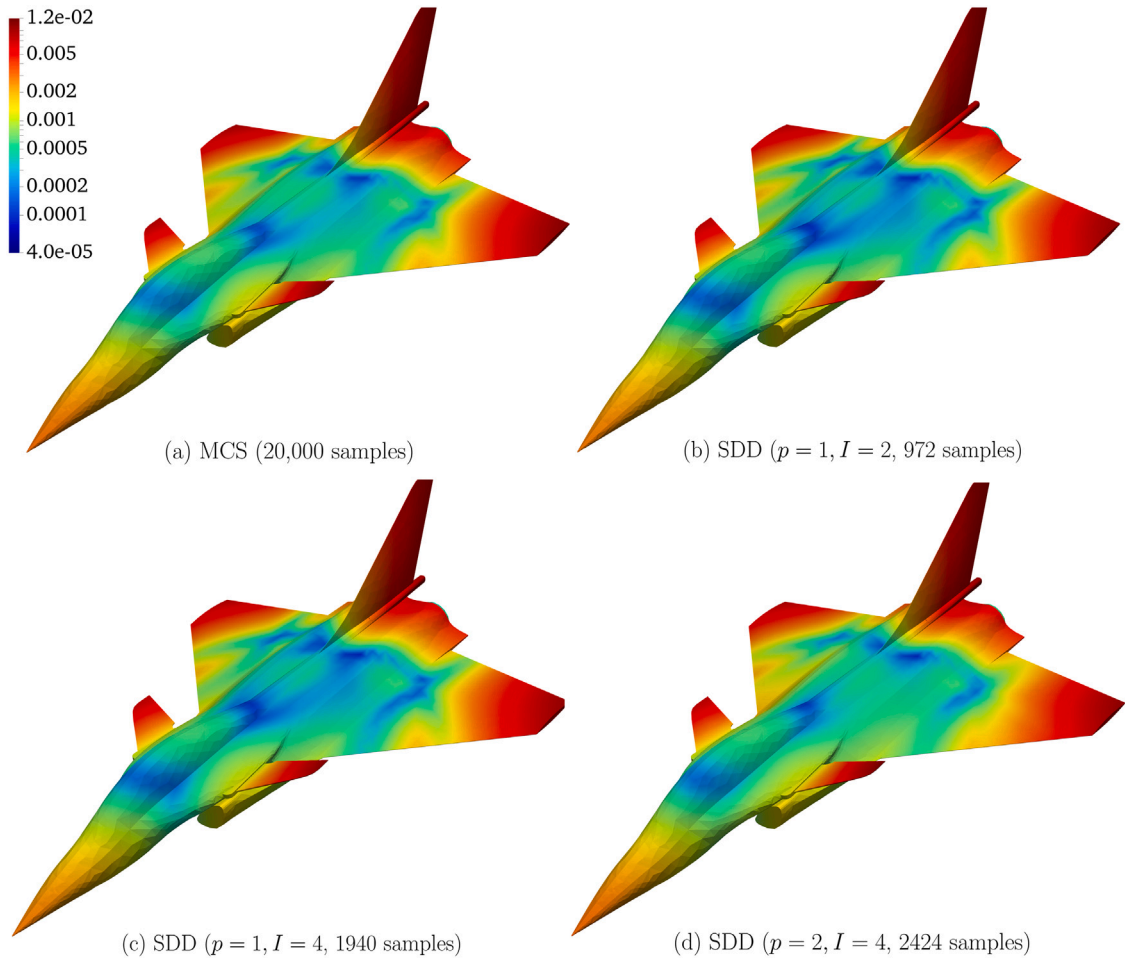


Fig. 8. Standard deviation contour plot of the sixth non-rigid-body mode shape.

8. Conclusion

Two novel spline expansions, designated as SCE and SDD, were studied for solving UQ problems commonly encountered in structural dynamics of linear systems. Both methods feature Fourier-like expansions of a dynamic system response of interest with respect to measure-consistent orthonormalized B-splines in input random variables and SLS regression for estimating the expansion coefficients. SCE is similar to PCE, but by swapping polynomials for B-splines, SCE achieves a greater flexibility in selecting expansion orders and dealing with subdomains. For this very reason, SCE can effectively tackle stochastic responses that contain locally high fluctuations and that are non-smooth. However, due to the tensor-product structure, SCE, like its polynomial sibling, suffers from the curse of dimensionality. This is chiefly because the number of SCE's multivariate B-splines grows exponentially with the number of input random variables. In contrast, SDD impedes the proliferation of the requisite number of such basis functions as much as possible while maintaining the desired accuracy in stochastic solutions. SDD accomplishes this task by exploiting multivariate B-splines in a progressive, dimensionwise way to create the resulting expansion. Consequently, SDD alleviates the curse of dimensionality to an appreciable magnitude.

Numerical results from frequency response analysis of a two-degree-of-freedom dynamic system indicate that a low-order SCE with fewer basis functions eliminates or substantially mitigates the spurious oscillations generated by high-order PCE in calculating the second-moment statistics and probability distributions of FRFs. A truly high-dimensional UQ problem, encompassing modal analysis of a fighter jet with 110 random variables, was solved by SDD and crude MCS. From the comparisons of results, SDD produces satisfactory estimates of the probabilistic characteristics of natural frequencies and mode shapes incurring less than ten percent of the computational effort by MCS. Therefore, SDD, unlike SCE, is capable of solving large-scale UQ problems from real-life applications.

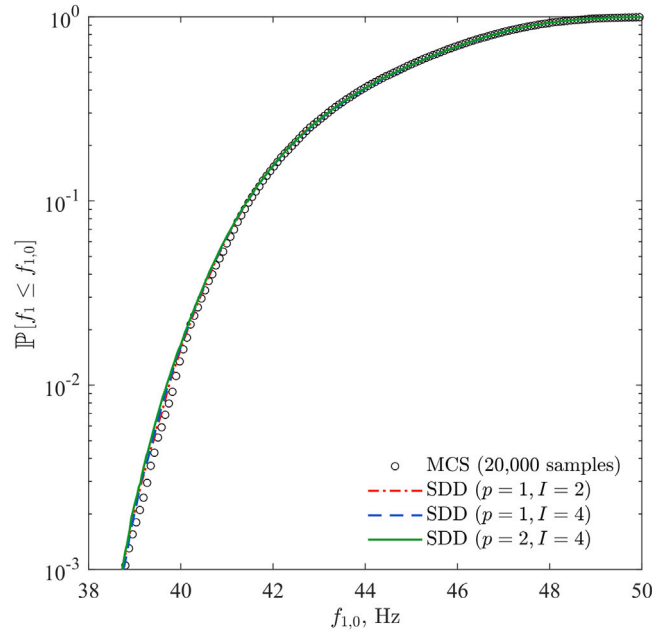


Fig. 9. CDF of the first non-rigid-body mode frequency.

CRedit authorship contribution statement

Sharif Rahman: Conceptualization, Methodology, Formal analysis, Writing – original draft, Supervision, Funding acquisition.
Ramin Jahanbin: Software, Verification, Formal analysis, Visualization, Data curation, Writing – review & editing.

Declaration of competing interest

The authors declare that they have no known competing financial interests or personal relationships that could have appeared to influence the work reported in this paper.

Appendix. Univariate B-splines

Let $\mathbf{x} = (x_1, \dots, x_N)$ be an arbitrary point in \mathbb{A}^N . For the coordinate direction $k, k = 1, \dots, N$, define a positive integer $n_k \in \mathbb{N}$ and a non-negative integer $p_k \in \mathbb{N}_0$, representing the total number of basis functions and polynomial degree, respectively. The rest of this appendix briefly describes paraphernalia of univariate B-splines.

A.1. Knot vector

In order to define B-splines, the concept of knot vector, also referred to as knot sequence, for each coordinate direction k is needed.

Definition 3. A knot vector ξ_k for the interval $[a_k, b_k] \subset \mathbb{R}$, given $n_k > p_k \geq 0$, is a vector comprising a non-decreasing sequence of real numbers

$$\xi_k := \{\xi_{k,i_k}\}_{i_k=1}^{n_k+p_k+1} = \{a_k = \xi_{k,1}, \xi_{k,2}, \dots, \xi_{k,n_k+p_k+1} = b_k\}, \tag{A.1}$$

$$\xi_{k,1} \leq \xi_{k,2} \leq \dots \leq \xi_{k,n_k+p_k+1},$$

where ξ_{k,i_k} is the i_k th knot with $i_k = 1, 2, \dots, n_k + p_k + 1$ representing the knot index for the coordinate direction k . The elements of ξ_k are called knots.

According to Eq. (A.1), there are a total of $n_k + p_k + 1$ knots, which may be equally or unequally spaced. To monitor knots without repetitions, denote by $\zeta_{k,1}, \dots, \zeta_{k,r_k}$ the r_k distinct knots in ξ_k with respective multiplicities $m_{k,1}, \dots, m_{k,r_k}$. Then the knot vector in

Eq. (A.1) can be expressed more compactly by

$$\xi_k = \{a_k = \overbrace{\zeta_{k,1}, \dots, \zeta_{k,1}}^{m_{k,1} \text{ times}}, \overbrace{\zeta_{k,2}, \dots, \zeta_{k,2}}^{m_{k,2} \text{ times}}, \dots, \overbrace{\zeta_{k,r_k-1}, \dots, \zeta_{k,r_k-1}}^{m_{k,r_k-1} \text{ times}}, \overbrace{\zeta_{k,r_k}, \dots, \zeta_{k,r_k}}^{m_{k,r_k} \text{ times}} = b_k\},$$

$$a_k = \zeta_{k,1} < \zeta_{k,2} < \dots < \zeta_{k,r_k-1} < \zeta_{k,r_k} = b_k,$$
(A.2)

which consists of a total number of

$$\sum_{j_k=1}^{r_k} m_{k,j_k} = n_k + p_k + 1$$
(A.3)

knots. As shown in Eq. (A.2), each knot, whether interior or exterior, may appear $1 \leq m_{k,j_k} \leq p_k + 1$ times, where m_{k,j_k} is referred to as its multiplicity. The multiplicity has important implications on the regularity properties of B-spline functions. A knot vector is called open if the end knots have multiplicities $p_k + 1$. In this case, definitions of more specific knot vectors are in order.

Definition 4. A knot vector is said to be $(p_k + 1)$ -open if the first and last knots appear $p_k + 1$ times, that is, if

$$\xi_k = \{a_k = \overbrace{\zeta_{k,1}, \dots, \zeta_{k,1}}^{p_k+1 \text{ times}}, \overbrace{\zeta_{k,2}, \dots, \zeta_{k,2}}^{m_{k,2} \text{ times}}, \dots, \overbrace{\zeta_{k,r_k-1}, \dots, \zeta_{k,r_k-1}}^{m_{k,r_k-1} \text{ times}}, \overbrace{\zeta_{k,r_k}, \dots, \zeta_{k,r_k}}^{p_k+1 \text{ times}} = b_k\},$$

$$a_k = \zeta_{k,1} < \zeta_{k,2} < \dots < \zeta_{k,r_k-1} < \zeta_{k,r_k} = b_k.$$
(A.4)

Definition 5. A knot vector is said to be $(p_k + 1)$ -open with simple knots if it is $(p_k + 1)$ -open and all interior knots appear only once, that is, if

$$\xi_k = \{a_k = \overbrace{\zeta_{k,1}, \dots, \zeta_{k,1}}^{p_k+1 \text{ times}}, \zeta_{k,2}, \dots, \zeta_{k,r_k-1}, \overbrace{\zeta_{k,r_k}, \dots, \zeta_{k,r_k}}^{p_k+1 \text{ times}} = b_k\},$$

$$a_k = \zeta_{k,1} < \zeta_{k,2} < \dots < \zeta_{k,r_k-1} < \zeta_{k,r_k} = b_k.$$
(A.5)

A $(p_k + 1)$ -open knot vector with or without simple knots is commonly found in applications [35]. However, only simple knots are used in this work.

A.2. B-splines

The B-spline functions for a given degree are defined in a recursive manner using the knot vector as follows.

Definition 6. Let ξ_k be a general knot vector of length at least $p_k + 2$ for the interval $[a_k, b_k]$, as defined by Eq. (A.1). Denote by $B_{i_k, p_k, \xi_k}^k(x_k)$ the i_k th univariate B-spline function with degree $p_k \in \mathbb{N}_0$ for the coordinate direction k . Given the zero-degree basis functions,

$$B_{i_k, 0, \xi_k}^k(x_k) := \begin{cases} 1, & \xi_{k,i_k} \leq x_k < \xi_{k,i_k+1}, \\ 0, & \text{otherwise,} \end{cases}$$
(A.6)

for $k = 1, \dots, N$, all higher-order B-spline functions on \mathbb{R} are defined recursively by

$$B_{i_k, p_k, \xi_k}^k(x_k) = \frac{x_k - \xi_{k,i_k}}{\xi_{k,i_k+p_k} - \xi_{k,i_k}} B_{i_k, p_k-1, \xi_k}^k(x_k) + \frac{\xi_{k,i_k+p_k+1} - x_k}{\xi_{k,i_k+p_k+1} - \xi_{k,i_k+1}} B_{i_k+1, p_k-1, \xi_k}^k(x_k),$$
(A.7)

where $1 \leq k \leq N$, $1 \leq i_k \leq n_k$, $1 \leq p_k < \infty$, and $0/0$ is considered as zero.

The recursive formula in Definition 6 was derived by Cox [45] and de Boor [36].

References

- [1] M. Grigoriu, Stochastic Calculus: Applications in Science and Engineering, Birkhauser, 2002.
- [2] T.J. Sullivan, Introduction To Uncertainty Quantification, Springer, New York, 1971.
- [3] N. Wiener, The homogeneous chaos, Amer. J. Math. 60 (4) (1938) 897–936.
- [4] R.H. Cameron, W.T. Martin, The orthogonal development of non-linear functionals in series of Fourier–Hermite functionals, Ann. of Math. 48 (1947) 385–392.
- [5] S. Rahman, A polynomial dimensional decomposition for stochastic computing, Internat. J. Numer. Methods Engrg. 76 (2008) 2091–2116.
- [6] S. Rahman, Mathematical properties of polynomial dimensional decomposition, SIAM/ASA J. Uncertain. Quantif. 6 (2018) 816–844.
- [7] I. Babuska, F. Nobile, R. Tempone, A stochastic collocation method for elliptic partial differential equations with random input data, SIAM J. Numer. Anal. 45 (3) (2007) 1005–1034.
- [8] B. Ganapathysubramanian, N. Zabarar, Sparse grid collocation schemes for stochastic natural convection problems, J. Comput. Phys. 225 (1) (2007) 652–685.

- [9] S. Smolyak, Quadrature and interpolation formulas for tensor products of certain classes of functions, *Dokl. Akad. Nauk SSSR* 4 (1963) 240–243.
- [10] T. Gerstner, M. Griebel, Numerical integration using sparse grids, *Numer. Algorithms* 18 (1998) 209–232.
- [11] R.Y. Rubinstein, D.P. Kroese, *Simulation and the Monte Carlo Method*, vol. 707, John Wiley & Sons, 2011.
- [12] H. Niederreiter, J. Spanier, *Monte Carlo and Quasi-Monte Carlo Methods*, Springer-Verlag: Berlin, 2000.
- [13] X. Wan, G. Karniadakis, Long-term behavior of polynomial chaos in stochastic flow simulations, *Comput. Methods Appl. Mech. Engrg.* 195 (2006) 5582–5596.
- [14] M. Gerritsma, J.B. Van der Steen, P. Vos, G. Karniadakis, Time-dependent generalized polynomial chaos, *J. Comput. Phys.* 229 (2010) 8333–8363.
- [15] V. Heuveline, M. Schick, A hybrid generalized polynomial chaos method for stochastic dynamical systems, *Int. J. Uncertain. Quantif.* 4 (2014) 37–61.
- [16] L. Pichler, H.J. Pradlwarter, G. Schueller, A mode-based meta-model for the frequency response functions of uncertain structural systems, *Comput. Struct.* 87 (2009) 332–341.
- [17] B. Van den Nieuwenhof, J.P. Coyette, Modal approaches for the stochastic finite element analysis of structures with material and geometric uncertainties, *Comput. Methods Appl. Mech. Engrg.* 192 (2003) 3705–3729.
- [18] A. Manan, J. J. Cooper, Prediction of uncertain frequency response function bounds using polynomial chaos expansion, *J. Sound Vib.* 329 (2010) 3348–3358.
- [19] A. Kundu, S. Adhikari, Dynamic analysis of stochastic structural systems using frequency adaptive spectral functions, *Probab. Eng. Mech.* 39 (2015) 23–38.
- [20] J. Jacquelin, S. Adhikari, J.J. Sinou, M.I. Friswell, Polynomial chaos expansion and steady-state response of a class of random dynamical systems, *J. Eng. Mech.* 141 (2015) Article 04014145.
- [21] J. Jacquelin, S. Adhikari, J.J. Sinou, M.I. Friswell, Polynomial chaos expansion in structural dynamics: accelerating the convergence of the first two statistical moment sequences, *J. Sound Vib.* 356 (2015) 144–154.
- [22] V. Yaghoubi, S. Marelli, B. Sudret, T. Abrahamsson, Sparse polynomial chaos expansions of frequency response functions using stochastic frequency transformation, *Probab. Eng. Mech.* 48 (2017) 39–58.
- [23] W.E. Boyce, Random eigenvalue problems, in: A. Bharucha-Reid (Ed.), *Probabilistic Methods in Applied Mathematics I*, v. 3, Academic Press, 1968.
- [24] S. Mehlhose, J. Vom Scheidt, R. Wunderlich, Random eigenvalue problems for bending vibrations of beams, *ZAMM, Z. Angew. Math. Mech.* 14 (1998).
- [25] M. Grigoriu, A solution of the random eigenvalue problem by crossing theory, *J. Sound Vib.* 158 (1) (1992) 69–80.
- [26] D. Ghosh, R.G. Ghanem, Analysis of eigenvalues and modal interaction of stochastic systems, *AIAA J.* 43 (10) (2005) 2196–2201.
- [27] S. Rahman, A solution of the random eigenvalue problem by a dimensional decomposition method, *Internat. J. Numer. Methods Engrg.* 67 (2006) 1318–1340.
- [28] S. Rahman, Stochastic dynamic systems with complex-valued eigensolutions, *Internat. J. Numer. Methods Engrg.* 71 (2007) 963–986.
- [29] R. Bellman, *Dynamic Programming*, Princeton University Press, Princeton, NJ, 1957.
- [30] S. Rahman, V. Yadav, Orthogonal polynomial expansions for solving random eigenvalue problems, *Int. J. Uncertain. Quantif.* 1 (2011) 163–187.
- [31] L.J. Schumaker, *Spline Functions: Basic Theory*, third ed., Cambridge University Press, Cambridge, 2007.
- [32] S. Rahman, A spline chaos expansion, *SIAM/ASA J. Uncertain. Quantif.* 8 (2020) 27–57.
- [33] S. Rahman, R. Jahanbin, A spline dimensional decomposition for uncertainty quantification, *SIAM/ASA J. Uncertain. Quantif.* (2020) (submitted for publication).
- [34] M. Hamadaoui, K. Akoussan, D. ElMostafa, Comparison of non-linear eigensolvers for modal analysis of frequency dependent laminated visco-elastic sandwich plates, *Finite Elem. Anal. Des.* 121 (2016) 75–85.
- [35] J.A. Cottrell, T.J.R. Hughes, Y. Bazilevs, *Isogeometric Analysis: Toward Integration of CAD and FEA*, John Wiley & Sons, 2009.
- [36] C. De Boor, On calculation with B-splines, *J. Approx. Theory* 6 (1972) 50–62.
- [37] R.E. Cafilisch, W. Morokoff, A. Owen, Valuation of mortgage backed securities using Brownian bridges to reduce effective dimension, *J. Comput. Finance* 1 (1997) 27–46.
- [38] R. Jahanbin, S. Rahman, Stochastic isogeometric analysis in linear elasticity, *Comput. Methods Appl. Mech. Engrg.* 364 (2020) 1–38, Article 112928.
- [39] Y. Audoux, M. Montemurro, J. Pailhes, Non-uniform rational basis spline hyper-surfaces for metamodelling, *Comput. Methods Appl. Mech. Engrg.* 364 (2020) 1–26, Article 112918.
- [40] S. Dixler, R. Jahanbin, S. Rahman, Uncertainty quantification by optimal spline dimensional decomposition, *Internat. J. Numer. Methods Engrg.* (2021) 1–37, <http://dx.doi.org/10.1002/nme.6778>.
- [41] H. Xu, S. Rahman, A generalized dimension-reduction method for multi-dimensional integration in stochastic mechanics, *Internat. J. Numer. Methods Engrg.* 61 (2004) 1992–2019.
- [42] Dassault Rafale jet, In wikipedia, 2021, Retrieved February 2021.
- [43] Dassault Systems Simulia Corp., *Abaqus standard*, version 6.9, 2019.
- [44] C. Lanczos, An iteration method for the solution of the eigenvalue problem of linear differential and integral operators, *J. Res. Natl. Bur. Stand.* 45 (1950) 255–282.
- [45] M.G. Cox, The numerical evaluation of B-splines, *J. Inst. Math. Appl.* 10 (1972) 134–149.